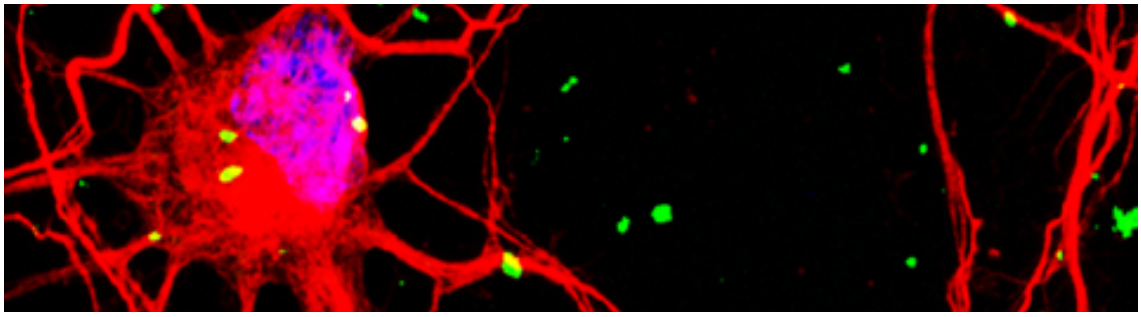

Corso di Dottorato in Neuroscienze
Curriculum Neuroscienze e Neurotecnologie
Ciclo XXX

GABAergic synaptic protein dynamics measured by spectroscopic approaches

Autore: Francesco Colaci
Supervisor: Andrea Barberis

ISTITUTO ITALIANO DI TECNOLOGIA

UNIVERSITÀ DEGLI STUDI DI GENOVA

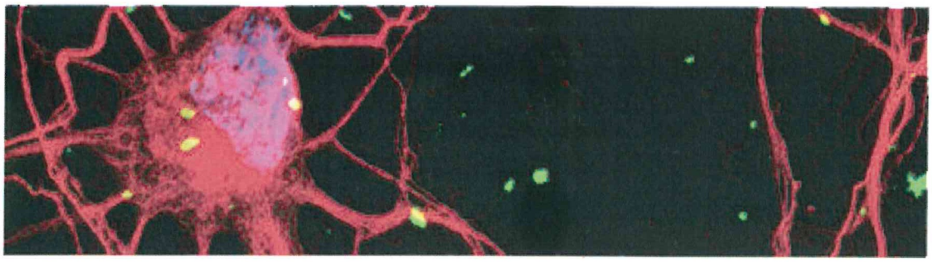

Corso di Dottorato in Neuroscienze
Curriculum Neuroscienze e Neurotecnologie
Ciclo XXX

GABAergic synaptic protein dynamics measured by spectroscopic approaches

Autore: Francesco Colaci
Supervisor: Andrea Barberis

Francesco Colaci

ISTITUTO ITALIANO DI TECNOLOGIA

UNIVERSITÀ DEGLI STUDI DI GENOVA

TABLE OF CONTENTS

LIST OF FIGURES

LIST OF ACRONYMS

AB	AntiBody
ACF	AutoCorrelation Function
AMPA	α-amino-3-hydroxy-5-methyl-4-isoxazolepropionic acid
ARICS	Arbitrary Region Raster Image Correlation Spectroscopy
Dex	Dextran
EGFP (GFP)	Enhanced Green Fluorescent Protein
FCCS	Fluorescence Cross-Correlation Spectroscopy
FCS	Fluorescence Correlation Spectroscopy
FRAP	Fluorescence recovery after photobleaching
FRET	Förster/Fluorescence Resonance Energy Transfer
GABA	γ-Aminobutyric acid
GABAAR	GABAA Receptor
GPHN	Gephyrin
HA	Hemagglutinin (influenza)
HEK	Human Embryonic Kidney cells 293
MSD	Mean Squared Displacement
N2A	Neuro2a cells (mouse neuroblastoma cell line)
Neu	Neuron
NMDA	N-methyl-D-aspartate
QD	Quantum Dot
RICS	Raster Image Correlation Spectroscopy
SPT	Single Particle Tracking
WT	Wild Type

ABSTRACT

The activity dependent adjustment of synaptic strength (synaptic plasticity) involves the reorganization of post-synaptic proteins. The fast diffusion of synaptic proteins has been shown to play an important role in such molecular rearrangements. Taking advantage of single particle tracking (SPT) and fluorescence recovery after photobleaching (FRAP) techniques, it has been demonstrated that during inhibitory long-term potentiation (iLTP) the scaffold protein gephyrin and GABAA receptors are accumulated and immobilized at post-synaptic inhibitory sites. However, the interaction and diffusion properties of gephyrin and GABAA receptors outside and inside the synapse remain to be elucidated. To investigate the dynamics of synaptic GABAergic proteins, in addition to Single Particle Tracking (SPT), we exploited two spectroscopic approaches based on Fluorescence Correlation Spectroscopy (FCS) and Raster Image Correlation Spectroscopy (RICS). In particular, FCS and RICS were optimized to study the coordinated multilevel organization of receptors that laterally diffuse on the plasma membrane and the scaffold proteins gephyrin that diffuse in the cytoplasmic space. Our data suggest that gephyrin freely diffuse in the extrasynaptic space and is suddenly immobilized at gephyrin clusters. However, inside the gephyrin clusters, a bimodal diffusion of gephyrin diffusion was observed, thus reinforcing an "aggregation-removal model" that ensure the plastic behaviour of the synapse. Furthermore, the surface lateral diffusion of GABAA receptors measured with the aforementioned spectroscopy techniques yielded similar values with respect to the more conventional quantum dots-based SPT, thus validating the use of FCS and RICS for the study of the diffusion of synaptic proteins. In summary, spectroscopy approaches may extend the study of fast molecular diffusion to intracellular proteins allowing, for instance, to investigate the coordinated diffusion of membrane synaptic proteins and scaffold proteins, thus clarifying the mechanisms of synaptic clustering in basal conditions and during synaptic plasticity at unprecedented resolution.

AIM OF THE THESIS

The main focus of this work is to understand the fine functioning of the synapse. In this frame, the role played by the diffusion of synaptic proteins remains unclear. We focused on the coordinated diffusion of the main proteins at the inhibitory synapse: the GABAergic receptors and the scaffold protein gephyrin.

Although several experimental approaches (quantum-dot based Single Particle Tracking, SPT) allows to measure the diffusion of transmembrane proteins, the characterization of intracellular dynamics of the cytosolic proteins can be achieved only with indirect or low spatio-temporal resolution measurements such as, for instance, Fluorescence Recovery After Photobleaching (FRAP). To overcome this issue, I employed innovative spectroscopy approaches with the ultimate goal to study the relation between the dynamics of cytoplasmic and membrane proteins.

For this purpose, I used Fluorescence Correlation Spectroscopy technique (FCS) and Arbitrary Region Correlation Spectroscopy technique (ARICS) on hippocampal cultured neurons focusing on the intracellular dynamics of gephyrin and the surface GABAA receptor lateral mobility. Both these spectroscopic approaches allow to simultaneously investigate the diffusion of particles both in the membrane and cytosolic sub-compartments, with substantially increased space-time resolution with respect to the FRAP technique. With respect to FCS, in particular, the ARICS approach allows the quantification of bulk particle diffusion also in the spatial domain by using conventional confocal scanning microscopy. The diffusion values of surface GABAAR obtained with spectroscopic approach have been validated with those measured with the widely used technique of the quantum dot-based single particle tracking, thus indicating that spectroscopy is a suitable tool for the characterization of protein diffusion in specific cellular domain.

Currently, I'm optimizing Fluorescence Cross-Correlation Spectroscopy (FCCS) to achieve a more quantitative insight on the simultaneous membrane and cytosolic protein dynamics to unveil the coordinated diffusion dynamics at synaptic level.

In the future, I would like to combine these spectroscopic approaches with the Förster Resonance Energy Transfer (FRET) in order to measure the diffusion properties of interacting proteins dynamics.

INTRODUCTION

The dynamic synapse is the elementary functional unit of the network

A multitude of different stimuli are continuously received, processed and integrated in the nervous system, allowing every living organism to relate to itself and its environment.
This complex system gives to living organisms the ability to perceive, to process and react to external stimuli. The huge amount of data to be handled requires the coordination of an equally huge number of various events and processes, both at cellular and network levels. This extremely complex system regulation occurs at the level of synapse.
Synapses, from Greek ‘’*synapsis”* (*συνάψις*), meaning "conjunction", (from *συν,* "together" and *ἅπτειν,* "to fasten"), are highly specialized structures that connect and tune the interactions between neurons, producing a wide communication network based on synaptic circuits. The enormous complexity of the whole circuit is given by number, localization and by functional properties of individual synapses, enabling data processing through a high computational power. The brain contains more than one hundred billion of neurons, each of which builds and gets a variable number of synapses, from a few hundred to hundred thousand, amounting to an astronomical number of contacts and interactions. Neurons can be classified in various types defined by characteristic connectivity patterns. Furthermore, different morphological and molecular features, typical of inhibitory and excitatory synapses, can be distinguished at the synaptic level. Synapses are intercellular junctions extremely specialized and dynamics that connect pre- and post-synaptic neurons or pre-synaptic neurons to non-neuronal post synaptic effectors, like muscle cells.

Since the synaptic junctions are intercellular junctions, they are connected by the typical membrane specialized proteins that keep the space equally distributed between the two terminals, creating a structural connection between adjacent cells, the synaptic cleft (20-40 nm).
However, unlike common intercellular junctions, the pre and the post synaptic elements significantly differ in terms of structure and molecular organization. The reason of this is that they consist of two areas which are extremely specialized, on one side a pool of exocytotic vesicles (pre-synaptic) and, on the other, a cluster of high density receptors and scaffold proteins (post-synaptic).

Role of Inhibitory neurons in the neuronal network

Although the population of inhibitory neurons is smaller (15-20%) with respect to the total neuronal population in the Central Nervous System (CNS), there are believed to control the whole neuronal network (Somogyi, Fritschy, Benke, Roberts, & Sieghart, 1996). Interneurons are involved in dendritic integration of synaptic inputs and in the generation of rhythmic activity (M. Bartos et al., 2002; Marlene Bartos, Vida, & Jonas, 2007; Klausberger & Somogyi, 2008; Sohal, Zhang, Yizhar, & Deisseroth, 2009; Somogyi, Fritschy, Benke, Roberts, & Sieghart, 1996). The so far identified twenty-one subclasses of GABAergic interneurons found in the CA1 hippocampal region show specific biochemical, morphological and electrophysiological characteristics. The activity of inhibitory neurons has been shown to operate a fine control of pyramidal cell excitability, thus inducing specific network activity patterns that are believed to be crucial for the generations of brain states linked to the higher cognitive brain functions. This cell-type variability coordinates the network activity (Freund & Buzsáki, 1996; Klausberger & Somogyi, 2008) also through specific innervations of excitatory principal cells pyramidal neuron sub-regions such as proximal or distal dendrites, soma or axons (Klausberger & Somogyi, 2008). Examples of this concept are the input dendritic signalling of interneurons, that target the pyramidal cells on dendrites, where they can strongly affect glutamatergic dendritic inputs, playing a fundamental role in the neuronal integration

(Freund & Buzsáki, 1996). On the contrary, interneuronal inputs on the soma or the axon the pyramidal neurons are strategically located to control or "gate" the firing of action potentials. Interestingly, the compartmentalization of the inhibitory inputs on the dendritic tree matches that of excitatory inputs, thus indicating a high level or "local" coordination between excitation and inhibition (Klausberger & Somogyi, 2008; Spruston, 2008).

Gephyrin: the main scaffold protein at inhibitory synapses

Gephyrin is a 93 kDa protein purified in association with glycine receptor (GlyR) and co-purified with tubulin in the polymerized state (Choii & Ko, 2015). Due to these interactions, it was thought to be an anchoring protein for inhibitory receptors.

In vertebrates, gephyrin is made up of three fundamental domains: (1) the N-terminal G domain trimerization motif; (2) the central C-linker domain, that contains many residues site of post-translational modification and (3) the C-terminal E domain dimerization motif.

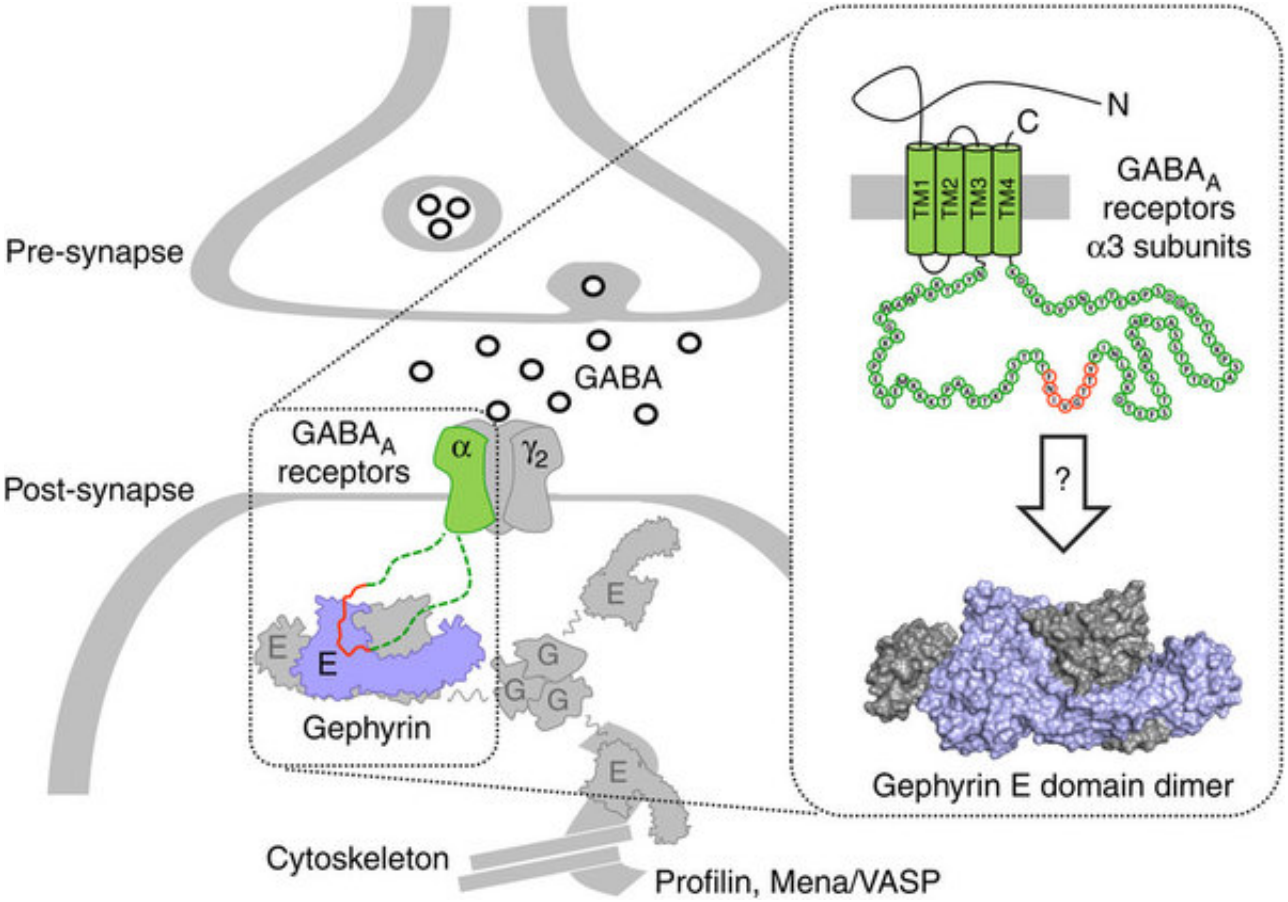

Figure 1 - Gephyrin organization in several aggregation states.

The aggregation of gephyrin occurs by dimerization of E domains and trimerization of G domains which triggers the formation of hexametric or multimeric aggregates. GABAARs containing α subunits directly engage the E domain (PDB entry 4PD0) near the dimer interface (dashed boxes). Gephyrin binding tethers the receptors to the cytoskeleton by direct interaction with profilin and Mena/VASP.
[from: (Maric et al., 2014)*]*

Gephyrin shows similarity with the invertebrate proteins involved in the molybdenum cofactor biosynthesis (Kamdar, Shelton, & Finnerty, 1994). In fact, G and E domains are respectively homologous to the Escherichia coli enzymes MogA and MoeA. These data are also confirmed by crystal structure analysis of gephyrin trimeric N-terminal domain (María Sola, Kneussel, Heck, Betz, & Weissenhorn, 2001).

The E domain specific sequences are crucial for the modulation of cytosolic aggregation and consequently postsynaptic receptor clustering. The gephyrin polymerization was also found to occur spontaneously, independently from external elements (Lardi-Studler et al., 2007).

Furthermore, crystal analysis of single domains unveils that the dimerization of E domains and trimerization of G domains may trigger the formation of multimeric hexagonal shaped aggregate (Kneussel & Betz, 2000).

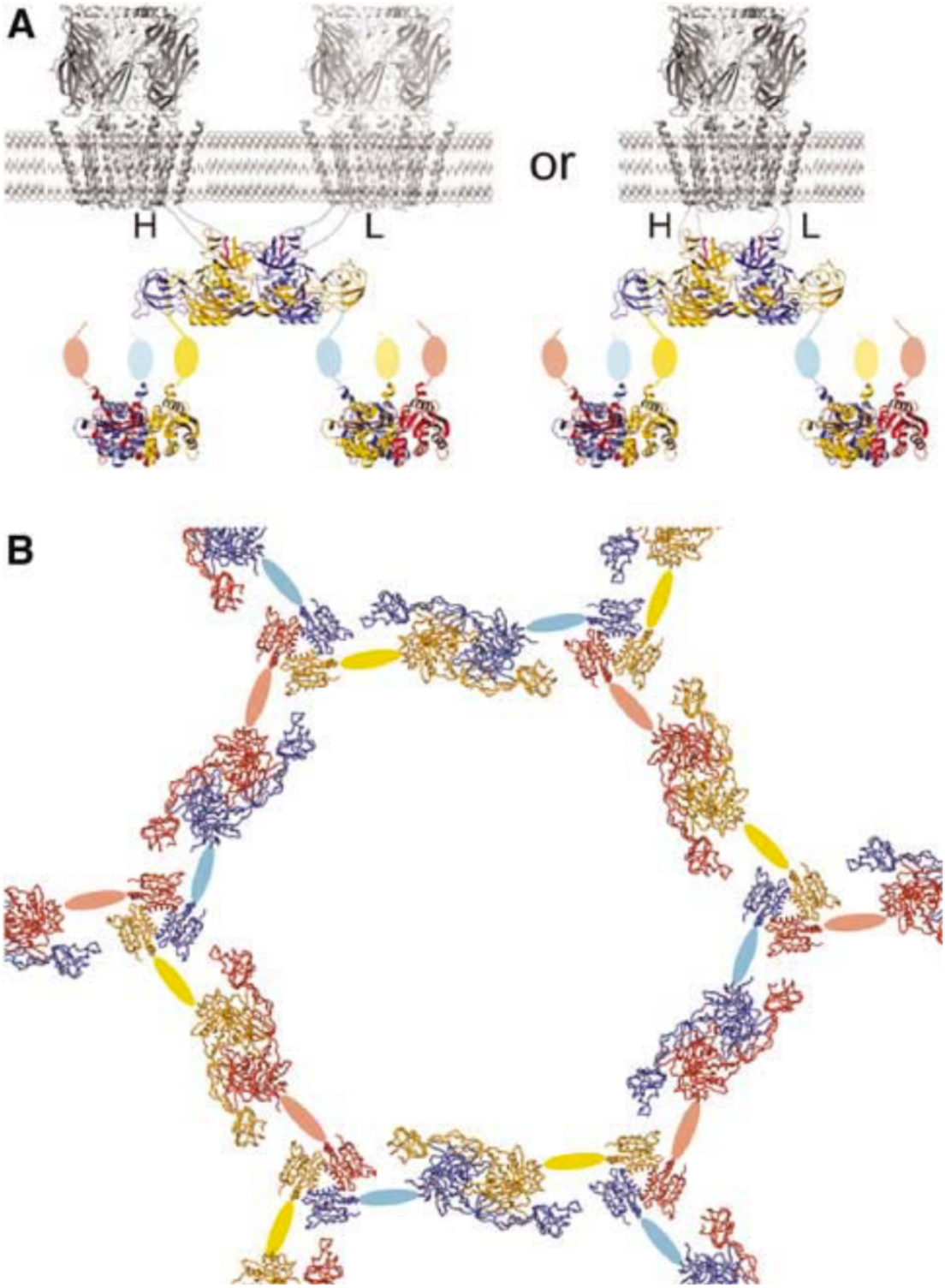

Figure 2 – Example of model for network formation and GlyR docking by gephyrin.

(A) The E-domain dimer might either interact with β- subunits from two different GlyR receptors (left panel) or with two β-subunits derived from one GlyR receptor (right panel). High- and low-affinity interactions with GlyR β-subunits are indicated (H, L).
(B) E-domain dimerization could potentially form a hexagonal network as viewed from the top. The G- and E-domains are shown as ribbon and the intermediate domain is drawn schematically. Each monomer chain is color coded differently.
[from: (Maria Sola et al., 2004)*].*

The oligomerized states of gephyrin are thought to initiate gephyrin aggregation in the sub-membrane space, where they can act as "anchoring sites" (Figure 2) (Maria Sola et al., 2004). Recent molecular studies demonstrated that splicing variants can lead to hexameric complexes with different stability levels (Herweg & Schwarz, 2012).

Moreover, the role of gephyrin in the inhibitory plasticity is mainly due to the convergence of several interactions, modifications and signalling pathways converging onto this protein. In fact, gephyrin is modulated by different signalling molecules, such as Ca^{2+}/calmodulin-dependent protein kinase II (CaMKII), extracellular signal–regulated kinases 1/2 (ERK1/2) and glycogen synthase kinase 3β (GSK3β). Moreover, gephyrin interacts with GABAA receptors (GABAAR) containing α1, α2, α3 subunit (Shiva K Tyagarajan & Fritschy, 2014) and additionally it binds directly to β2 and β3 subunits (Kowalczyk et al., 2013). Different signal transduction pathways impact on the post-translational modification of gephyrin, leading to a change of protein network at synapse (Ghosh et al., 2016). Phosphorylation of different residues, for example, is mediated by alternative pathways that can cause either reduced or enhanced inhibitory effect. The addition of phosphoryl group to the residue S270 due to the activity of GSK3β cause the destabilization of gephyrin clusters by the Ca^{2+}-dependent protease calpain-1 (S. K. Tyagarajan et al., 2011). A similar effect, functionally related to the previous, is caused by the phosphorylation of S268 by ERK1/2 (Shiva K. Tyagarajan et al., 2013). On the contrary, the NMDA receptor activity triggers the calcium dependent activity of CaMKII, causing the phosphorylation of the S383 residue of GABAA β3 receptor subunit. This modification strongly impacts on the synaptic recruitment of gephyrin that brings to the transient stabilization of GABAA receptors, as confirmed by quantum dot based single particle tracking experiments (Petrini et al., 2014). Therefore, the CamKII plays a crucial function during excitatory plasticity (Lisman, Yasuda, & Raghavachari, 2012) thus homeostatically balancing inhibitory synaptic plasticity (Flores et al., 2015).

Regarding the oligomerization states of gephyrin, a recent study shows a possible "aggregation-removal" model for the post-synaptic scaffold gephyrin domain (Ranft, Almeida,

Rodriguez, Triller, & Hakim, 2017). They assumed that the minimal gephyrin "building block" is the trimeric form (Belaidi & Schwarz, 2013; Schrader et al., 2004), and they obtained an average size for the gephyrin domain of N≈70 trimers (210 monomers) obtained by the balancing of the diffusion and aggregation gephyrin elementary blocks (Ranft, Almeida, Rodriguez, Triller, & Hakim, 2017).

The GABAergic synaptic transmission

The γ-aminobutyric acid (GABA) is the main inhibitory neurotransmitter in the mammalian brain (Nicoll, Malenka, & Kauer, 1990) and the most abundant in the whole central nervous system (Sivilotti & Nistri, 1991) where it mediates signals through GABAA and GABAB receptors. The synthesis starts from the decarboxylation of glutamate to GABA and carbon dioxide by glutamic acid decarboxylase (GAD) enzyme. GABA, like other neurotransmitters, once synthesized, is stored in the synaptic vesicles by the specific vesicle GABA transporter (vGAT) (McIntire, Reimer, Schuske, Edwards, & Jorgensen, 1997), which can be used as a presynaptic marker of GABAergic inhibitory synapses.

Vesicular release is modulated by several factors, including calcium release by intracellular stores and calcium-dependent calcium channels. Once released, GABA diffuses through the synaptic cleft in an extremely short time (~ 100μs). This fast diffusion is due to the very high density of neurotransmitter concentration inside the presynaptic vesicles (1-3mM) and the short distance between the pre and the post-synaptic element (~20 nm) (Mayer, 2006). Once reached the opposite side, GABA binds the postsynaptic receptors and, depending on the membrane concentration and the GABAA receptor subtype presence, induces a postsynaptic current showing different polarity, amplitude and duration.

The GABAA receptors

There are two different types of GABA receptors at the level of neuronal network: GABAA and GABAB, which differ in molecular structure, signal transduction mechanism, function and localization. The GABAC, containing rho subunit, are expressed at the level of vertebrate retina. GABAA receptors mediate rapid inhibitory action due to their ionotropic nature, while GABAB receptors are coupled to inhibitory G proteins and mediate slow synaptic inhibition (slower than 100 milliseconds). GABAA receptors are fast ionotropic receptors activated by ligand and permeable to chloride ions.

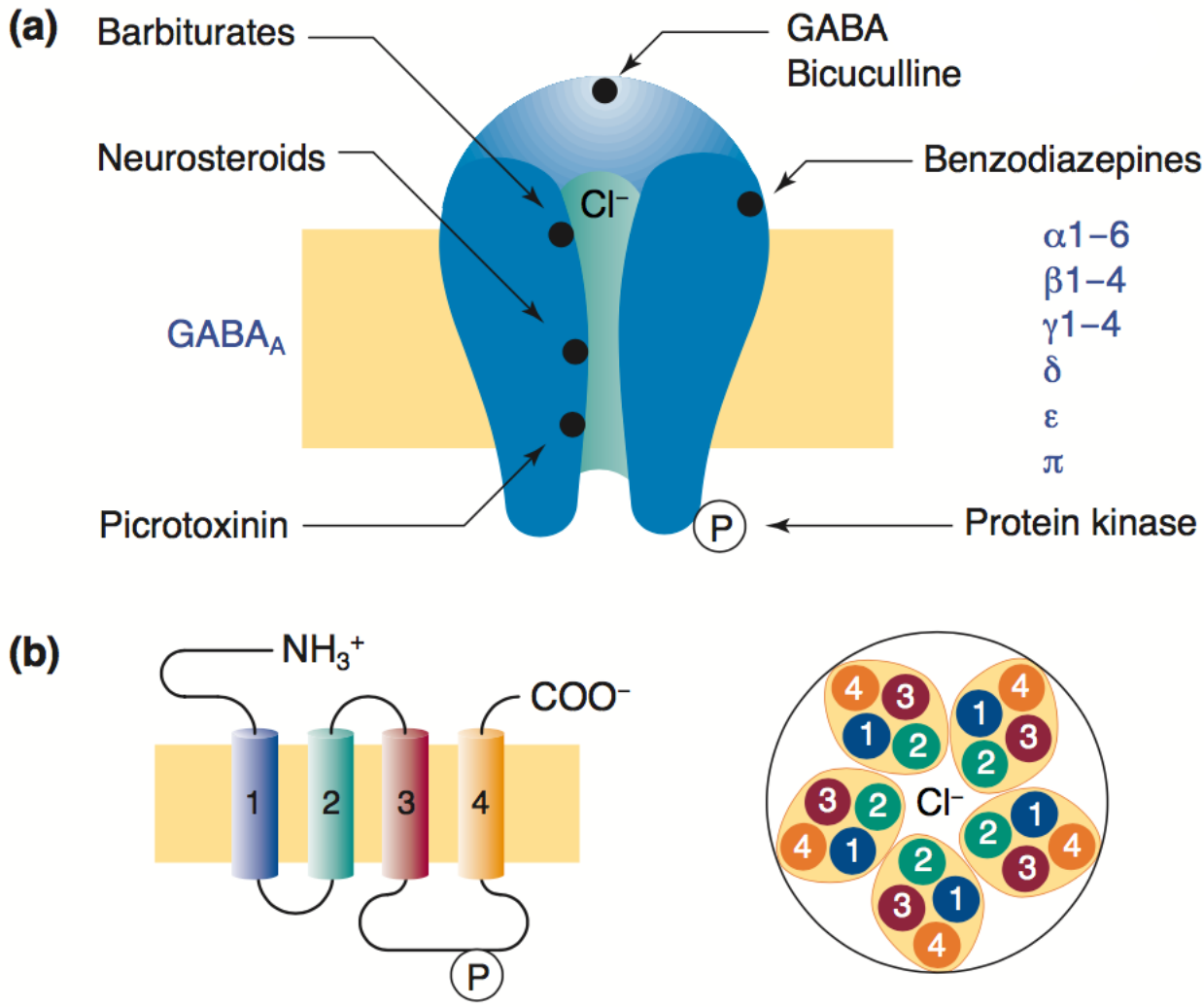

Figure 3 - GABAA receptor and binding sites.

(a) Schematic structure of the GABAA receptor with the main binding and allosteric sites.
(b) Scheme of a typical conformation of the GABAA receptor, consisting of an extracellular N-domain, 4 transmembrane segments (TM1-4) including the chloride permeable channel pore (TM2), the intracellular loop and a small extracellular C-terminal domain. [from: (Bormann, 2000)*].*

GABAA receptors have been identified based on their pharmacological profile: they are activated by γ-aminobutyric acid and by the muscimol agonists, while they are blocked by bicuculline and picrotoxin. Moreover they are also modulated by various pharmacological agents including benzodiazepines (BDZ), barbiturates and some anaesthetics (Macdonald & Olsen, 1994).

GABAARs are heteropentamers, assembled by 19 different subunits α (1-6), β (1-3), γ (1-3), δ, and ρ (1-3); a further difference among the subunits originates from the alternative splicing pattern. Each subunit consists in a large N-terminal extracellular domain, four transmembrane

domains (TM1-TM4), an intracellular loop between TM3 and TM4, and a small extracellular C-terminal domain. The N-terminal domain on the extracellular surface contains the signal peptide, a cysteine bridge and several glycosylation sites, while the TM3 and TM4 loop contains phosphorylation sites for protein kinase A (PKA), protein kinase C (PKC) and for tyrosine kinase (TrK). Through these sites the GABAA receptor may be regulated by phosphorylation of the various subunits, resulting in a reduction in chloride conductance and an increase in the desensitization rate. TM2 domain is crucial for receptor opening and selectivity: this portion defines the channel pore and constitutes the most conserved region. GABAA receptors may potentially be assembled in thousands of different combinations, nevertheless some studies have shown that only few subunit combinations are functionally expressed in the brain (Moss & Smart, 2001). Most GABAA receptors are formed by two copies of a α subunit, two copies of a β subunit, and a single subunit, typically represented by γ, δ or ε. The most common combination in the central nervous system is 2α, 2β and 1γ and is also the most abundant in hippocampal interneurons (Gao & Fritschy, 1994).

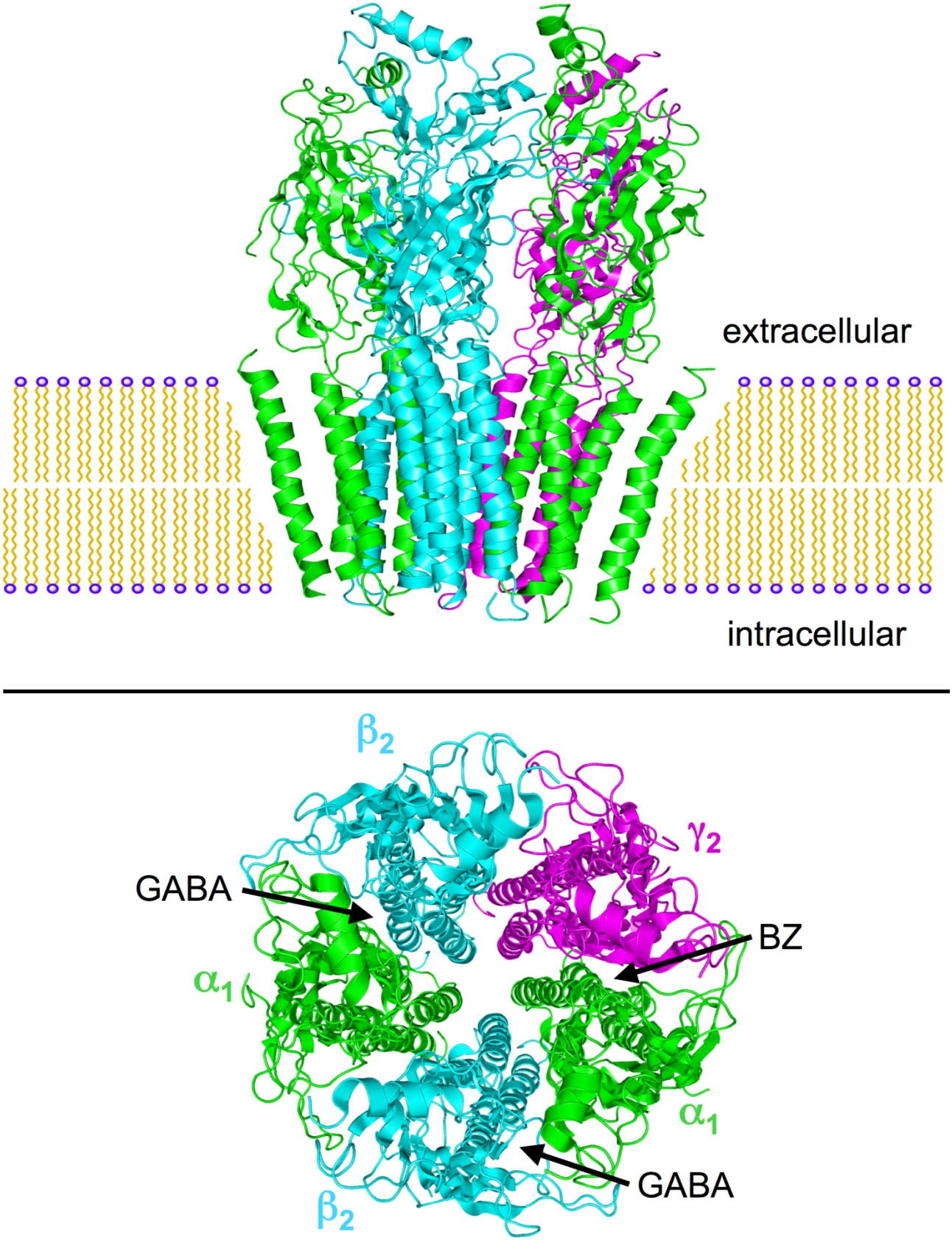

Figure 4 - Structural representation of the GABAA 2α1-2β2-1γ2 receptor, the most common assembly in the nervous system.

GABA interacts with the site formed between the α and β subunits, while BDZ links the allosteric site formed by the interface between α and γ subunits
(Thanks to: Boghog user - Wikipedia)

The different composition of the GABAA receptor determines fundamental functional properties such as pharmacological sensitivity, affinity, efficacy, kinetics and susceptibility to signalling pathways (Cherubini & Conti, 2001). The α subunit, for example, plays a crucial role in receptor kinetics: the presence of α1 and α3 leads respectively to fast or slow desensitization kinetics, while α2 kinetic cause an intermediate speed (Vicini et al., 2001) (Barberis, Mozrzymas, Ortinski, & Vicini, 2007). The subunits α4 and α6 are preferentially associated with the δ subunit, forming a receptor with a slow kinetics typically mediating tonic currents (Haas & Macdonald, 1999). In addition, the presence of the γ subunit strongly influences the pharmacological profile of the GABAA receptor and is necessary for benzodiazepine sensitivity (BDZ), as well as reducing the zinc ion blockage (Zn^{2+}). The presence of the δ subunit is a prerequisite for the sensitivity of GABAA to ethanol and to neurosteroids, while the response to benzodiazepines is effectively mediated by α1, α2, α3 and α5 subunits, but not by α4 and α6 which are insensitive to benzodiazepines. The effects of interaction of the different α subunits with BDZs are, however, extremely different: α1 causes an hypnotic effect, while α2 and α3 mediate an anxiolytic effect, underlining the fact that different receptor subtypes are involved in specific circuits (Olsen & Sieghart, 2009). Among the effects due to the α subunits of GABAA there is the anterograde amnesia caused by specific agonists of the α5 subunit, which is mainly expressed in the CA1 area of the dentate gyrus. Even more interesting is the effect of inverse agonists on this subunit: in fact, *in vivo* studies on rodent models have shown that the administration of selective inverse agonists of the α5 subunit improves the performance in dependent learning and memory tests in hippocampus, resulting in an improvement of cognitive abilities (Dawson et al., 2006).

The lateral mobility of GABA A receptors

In 2002, there was the first observation of single receptor lateral diffusion on the plasma membrane (Borgdorff & Choquet, 2002; Fernandes, Berg, & Gomez-Varela, 2010; Meier, Vannier, Sergé, Triller, & Choquet, 2001; Tardin, Cognet, Bats, Lounis, & Choquet, 2003a; Tovar & Westbrook, 2002). The concept of synapse has changed passing from a static condition with the receptor on the postsynaptic plasma membrane fixed in front of the presynaptic terminal, to a dynamic model governed by lateral diffusion of semi-permanent synaptic elements that continuously change their position and number. Postsynaptic receptors can freely diffuse, powered by thermal agitations (Brownian motion), and can be transiently slowed down by the scaffold proteins below the plasma membrane, typically at the synapse.

This new model is also influenced by lipid composition of the membrane and protein molecular crowding both at the level of membrane and cytoplasm, resulting in a heterogeneous environment and complex dynamics (Owen, Williamson, Rentero, & Gaus, 2009; Renner, Specht, & Triller, 2008). The diffusion rates observed in the extrasynaptic zones are in the range of 10^{0}-10^{1} μm2/s; on the contrary, in the synaptic areas the receptor dynamics are slowed down to 10^{-1}-10^{-3} μm2/s, mainly due to the diffusion traps (Petrini et al., 2009). The main source of transient stabilization of receptors at the synapses is the scaffold proteins, at both excitatory and inhibitory synapses. This mechanism was first identified by Meier et al. in 2001, in which the dynamic interaction between gephyrin and the β subunit of glycinergic receptors (GlyR) was shown at the inhibitory synapse of spinal cord neurons. In many following works, the interaction gephyrin-GABAAR, Homer-mGluR (Sergé, Fourgeaud, Hémar, & Choquet, 2002), stargazin-PSD95-AMPAR, SAP102-D1 receptors (Thurner et al., 2014) were demonstrated to stabilize receptors at the synapse. In particular the interaction between the GABAA receptor α1 subunit and the intracellular loop (TM3-4) of gephyrin E domain decreases the diffusion coefficient of receptor, causing a higher dwell time and an accumulation of GABAAR to the synaptic site; this finding was

also crucial to relate this mechanism to the inhibitory synaptic plasticity (Mukherjee et al., 2011). Many other GABAA receptor subunits are involved in the direct interaction with gephyrin creating a physical condition for the reversible "stop and go" mechanism, such as α2, α3, β2–3 and γ2 (Kowalczyk et al., 2013; Mou, Dias, Gosnell, & Ressler, 2013; Mukherjee et al., 2011; Tretter et al., 2008). The interaction affinity between gephyrin and GABAA receptor increases 25 times when the dimeric receptor fragments is bound to the dimeric gephyrin, with respect to the monovalent condition (Maric et al., 2014). The ratio between the oligomerization of gephyrin and the clusterization of receptors can potentially modulate the strength of inhibitory "diffusion trap" and the different subunits composition of the GABAA receptor can represents a further level of regulation of this model. The modulation levels are of two types: from one side the number of potential gephyrin-binding domains (4 in a typical combination of GABAAR αβγ) and, to the other side, the oligomerization state of gephyrin, from dimers or trimers to multimers. In this context, the receptor-scaffold transient interaction has been modelled assuming three conditions: (a) the formation of scaffold-receptor complex can exist both at the synaptic and extrasynaptic zones; (b) the synapse can be crossed by scaffold-receptor complexes, but receptor can also reach the synapse "alone"; (c) the scaffold-receptor interaction principally cause the receptor stabilization. The size of synaptic cluster, in the aforementioned model, is determined by a dynamic equilibrium between two opposite forces: receptor-receptor repulsions and scaffold-scaffold aggregations (Haselwandter, Calamai, Kardar, Triller, & Azeredo Da Silveira, 2011).

Mobility in the plasmatic membrane

Since the model by Singer and Nicolson presented at the beginning of the 70s, the plasmatic membrane has been described as an oriented system with transmembrane proteins in a dense phospholipidic bilayer (Singer & Nicolson, 1972). Nevertheless, the diffusion coefficients of lipids and proteins measured inside biological membrane were more than one order of magnitude lower compared to the results obtained on a lipid bilayer built in laboratory. Considering temperature almost constant in a biological system, the protein diffusion coefficients extracted from cellular membranes shown one order of magnitude lower than expected. This effect can be explained by the interaction with obstacles inside the membrane. At this meso-nanoscopic length scale the plasmatic membrane proteins passively diffuse and spread in different directions by thermal energy and molecular forces are ruled by viscous forces, making mass and inertia negligible.

Since Brownian motion is “random”, the prediction of the receptors position can only be determined by assuming a certain probability. In general, the diffusion of a molecule can be described by calculating the Mean Square Displacement versus time curve (MSD), that appears to be linear in time for the Brownian motion while reaches a steady state level in conditions of “confined mobility”

Single Particle Tracking (SPT)

The possibility to tether fluorophores to receptors allowed to display receptors diffusion at single molecule level in living cells. The accuracy achieved unveiled the variety of molecular motions, not only Brownian motion, but also constrained or oriented motion (Li, Xing, Qiu, He, & Lin, 2016; Qian, Sheetz, & Elson, 1991; Simson et al., 1998) The use of SPT technique for the study of molecular dynamics in live cells has been allowed, by two main technological advances that involved i) the development of new reporters for the receptor positions and the ii) optical detection of such reporter. Indeed latex/silicon micro particles (0,1 μm-1μm) or gold nanoparticles (≈40 nm), were replaces by Quantum dots (QD), fluorescent nanocrystal representing an optimal trade-off between brightness, photostability and size. The development of fluorescence microscopy and the enhancement of Charge-Coupled Device (CCD) Camera led to a remarkable sensitivity improvement and to the detection of single fluorophores in living cells (Moerner, 1999).

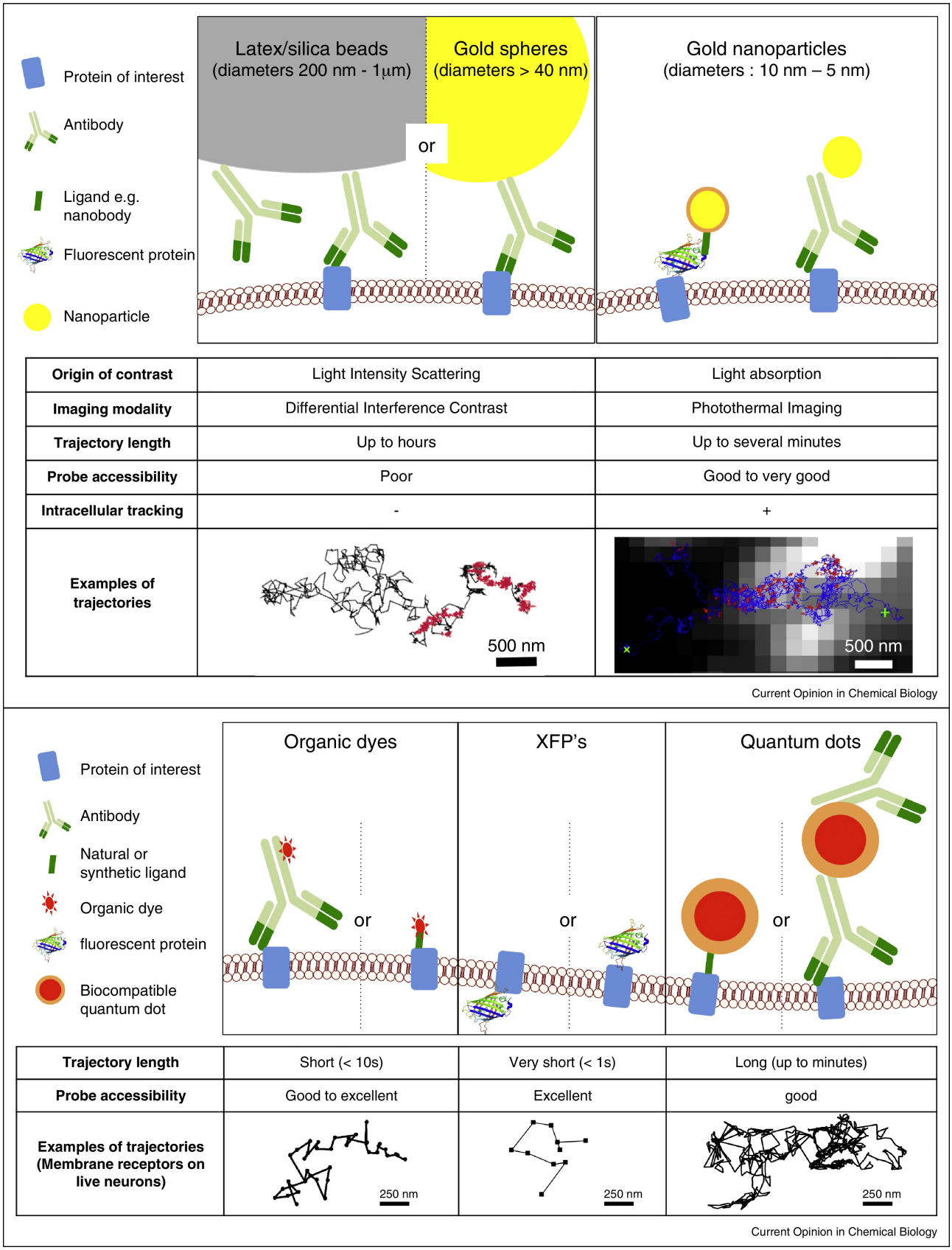

Origin of contrast	Light Intensity Scattering	Light absorption
Imaging modality	Differential Interference Contrast	Photothermal Imaging
Trajectory length	Up to hours	Up to several minutes
Probe accessibility	Poor	Good to very good
Intracellular tracking	-	+
Examples of trajectories		

Trajectory length	Short (< 10s)	Very short (< 1s)	Long (up to minutes)
Probe accessibility	Good to excellent	Excellent	good
Examples of trajectories (Membrane receptors on live neurons)			

Figure 5 - Single particle tracking detection systems.

Examples of reading systems: form latex beads, extremely bulky and inaccurate, to gold nanoparticles, quite accurate but rather big. Quantum dots offer high compatibility with biological systems and high signal/noise ratio.
In the lower areas examples of trajectories coming from the correspondent SPT detection system.
[from: (Cognet, Leduc, & Lounis, 2014)*].*

Organic fluorescent dyes like GFP allow an easy expression and coupling, they have a small size (< 1nm) and can be displayed in multicolour. The disadvantage of using them in the SPT measurements consists in a low fluorescence stability (fast photobleaching) that limits their use in SPT to few seconds (< 10s).

With the advent of the Quantum Dots (QDs), the SPT has reached a level of accuracy and ease of use that makes it the choice technique for lateral mobility study on the plasma membrane. Due to their photostability and their high quantum yields, QDs allowed measurement of individual receptors trajectories for prolonged acquisitions (even over an hour), with excellent signal-to-noise ratios.

QDs are luminescent semiconductor nanocrystals in colloidal solution. The core is covered by an inorganic semi conductive zinc sulphide shield (ZnS) necessary to increase the luminescence and an organic coating which makes the QD biocompatible, coming to thickness of 15-40 nm (Petryayeva, Algar, & Medintz, 2013). QDs show several advantages in terms of spectral properties: they are characterized by large excitation spectrum, and, conversely, a narrow, selective and symmetrical emission spectrum around a single wavelength. All of these features make them strongly suited to complex experimental conditions, for example, when the simultaneous use of different fluorophores is required in a multicolours image generated by a single excitation wavelength.

Furthermore, the possibility of high level of functionalization allows QDs to be selectively bound to target molecules of interest. The external shield can be designed to interact with the crystallisable region (Fc) of antibodies, thus allowing them to exploit their remarkable specificity.

From SPT to spectroscopy

Single particle tracking (SPT) is one of the most used technique to investigate protein surface dynamics in complex cellular systems. By estimating the trajectories of tagged particles, SPT allows to probe the behaviour of individual and tagged molecules. Nevertheless, to track individual molecules the density of probes conjugated to the labels must be kept very low. In addition inorganic probes (*e.g.,* quantum dots or gold nanoparticles), that are bright (allowing high temporal resolution in the μs range) and photostable (allowing to track the particle in the range of ten minutes), have to be conjugated with the molecule of interest with protocols that may alter the physiology of the cells (Di Rienzo, Gratton, Beltram, & Cardarelli, 2014).

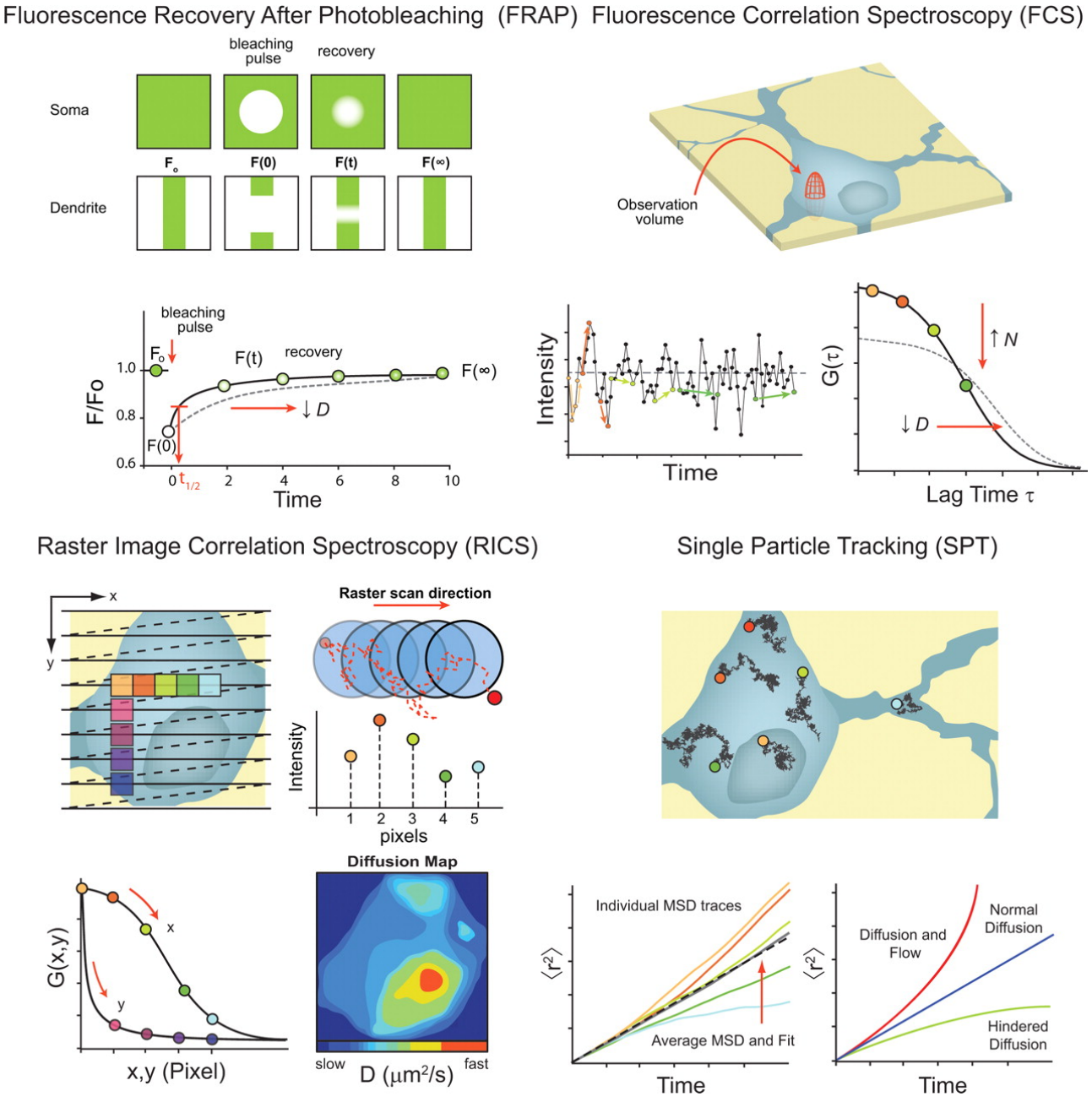

Figure 6 - Comparison of optical methods used for quantifying translational mobility in neurons.

[from: (Kim et al., 2010)*].*

Compared to SPT the spectroscopic methods, such as Fluorescent Correlation Spectroscopy (FCS) and Raster Image Correlation Spectroscopy (RICS), show some essential advantages. First of all, these approaches do not need the conjugated inorganic labelling: on the other hand, they allow the use of fluorescent proteins. Thus, due to the lower number of photons required, the temporal resolution reached is extremely higher, compared to the SPT, allowing to discriminate and scan an

extensive plethora of different fluctuations. In particular, this property allows pushing the temporal resolution below 10^{-4} s also when using fluorescent proteins. This timescale gives expanded access to the nanoscale dynamics of slow membrane dynamics and fast diffusion of cytoplasmic proteins as well. This extraordinary feature is useful to unmask protein dynamics invisible to other techniques, such as SPT or FRAP (Fluorescence Recovery After Photobleaching) and could become even more effective in revealing coordinated dynamics of different proteins with the Fluorescence Cross-Correlation Spectroscopy (FCCS) approach.

The spectroscopic approach extracts the biophysical parameters (diffusion coefficient and molecules concentration) from the diffusive behaviour of the entire detected particles population and does not need to track the particles trajectories, resulting in a less computational effort and easily automating processing (Di Rienzo et al., 2014).

Fluorescence Correlation Spectroscopy (FCS)

Various methods have been exploited in order to investigate the protein mobility. Fluorescence Correlation Spectroscopy, because of its numerous advantages, has been used to measure the dynamics of different proteins in living cells.

This technique, developed in the 70's (Magde, Elson, & Webb, 1972), measures the spontaneous fluctuation of fluorescence intensity in a small volume, allowing the study of molecular diffusion in a fluid system. Signal fluctuations arise because of the passive, thermally driven, motion of the molecules. If the number of molecules inside the illuminated open detection volume is small, as well as the volume itself, every single element passing through the volume drastically contributes to the fluorescence intensity signal.

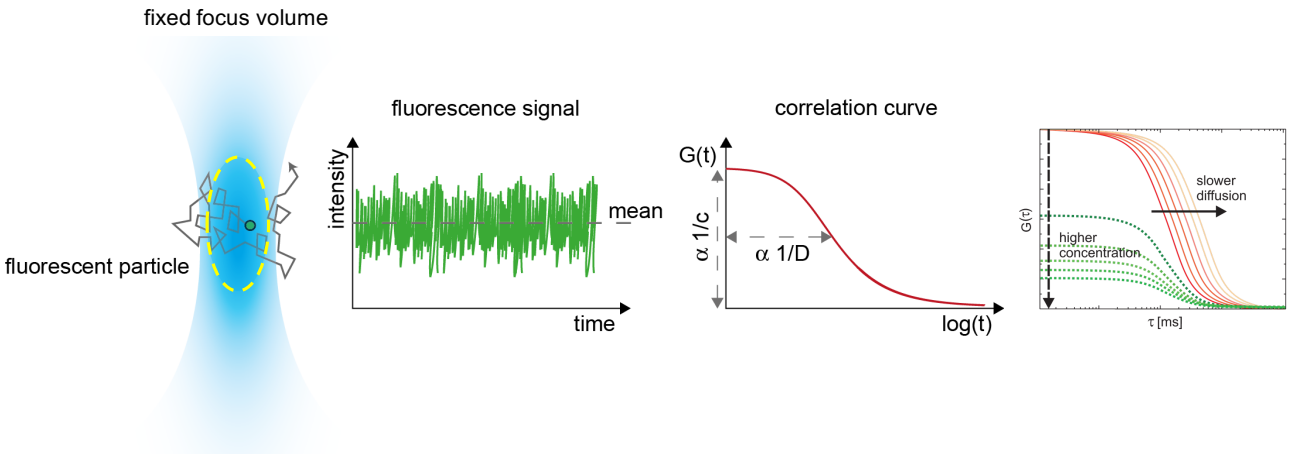

Figure 7 – Fluorescence Correlation Spectroscopy (FCS) analysis scheme.

The fluorescent proteins diffusing through the open detection volume (dashed ellipse) of a confocal microscope (fixed focus volume) give rise to intensity fluctuations trace (fluorescence signal). Then, the correlation curve is calculated as the autocorrelation of the intensity fluctuations thus measures the self-similarity of the signal. The amplitude of the autocorrelation curve is given by the inverse number of molecules in the detection volume, whereas its decay time reflects the diffusion coefficient of the protein.

The autocorrelation of the fluctuation is then computed in order to highlight temporal patterns that can be finally related to molecular dynamics, upon choice of the proper physical model. Practically, FCS allows to compute the diffusion coefficients of the interested molecules and their concentration. The major FCS advantages are high spatial resolution, fast temporal resolution and real-time computation of the diffusion parameters with only negligible perturbation of the sample. The main characteristics required in order to perform these measurements are: i) the ability of the system to illuminate just a very small volume (in the femtoliter range) ii) the number of molecules wandering in the volume must be very small, otherwise contributions to the fluctuation signal cannot be properly distinguished and, iii) the molecules must move (if they diffuse slow in the volume photobleaching becomes critical, distorting the results).

To perform these experiments, a laser with a high numerical aperture is used to excite the sample and the resulting emission of the fluorescent molecules in the open detection volume is collected. Once the fluctuation of the fluorescence intensity is computed also the autocorrelation function can be derived:

$$G(t) = \frac{\langle \delta F(t) \delta F(t+\tau) \rangle}{\langle F(t) \rangle^2},$$

where $F(t)$ is the fluorescence intensity, $\langle F(t)\rangle$ is the time average of the signal, $\delta F(t)$ is the fluctuation around the mean value and τ is the lag time.

The shape of the autocorrelation curve depends on the shape of the detection volume and on the fluorescent molecules.

In order to describe free diffusing molecules with a confocal detection volume a three-dimensional Gaussian profile is used:

$$G(\tau) = \frac{1}{N}\left(1 + \frac{\tau}{\tau_D}\right)^{-1}\left(1 + \frac{\tau}{S^2\tau_D}\right)^{-1/2}$$

In this case N is the average of particles in the volume, τ_D is the decay time (or diffusion time) that is related to the diffusion coefficient:

$\tau_D = \frac{w_0^2}{4D}$, where w_0 is the volume size.

The parameters of interest (N and τ_D, or more precisely D) are derived fitting the data collected during the experiments to the chosen form of the autocorrelation function.

Arbitrary Region Raster Image Correlation Spectroscopy (ARICS).

Image correlation spectroscopy (ICS) is an image processing method that, starting from a microscope single image or a stack, computes the spatial autocorrelation function which, once analyzed, provides information about number and size of aggregates. The rationale of this technique is that measured molecules are substantially not moving or slowly moving compared to the acquisition rate (seconds).

Raster Image Correlation Spectroscopy is placed in the middle between the low temporal resolution of ICS and the high temporal resolution of FCS, providing dynamic information in the microsecond to second time range. Experimentally, this method consists in acquiring a raster scan confocal image which will appear “striped” due to the different scanning speed of the confocal microscope along x and y directions and the motion of the fluorescent probes. Successively we compute the

autocorrelation function of the image which contains information about concentration and diffusion of the probes, that can be quantified by fitting it to a theoretical function. In order to increase the precision of RICS, we acquire several images of the same region and we average the autocorrelation functions, therefore obtaining a more robust fit.

It is important to discard the immobile fraction before computing the ACFs, otherwise it will artefactually contribute to the measurement of the spatial autocorrelation. This is done by subtracting from each image of the stack the temporal average of all the images and adding a constant background.

RICS results are significantly less influenced by photobleaching (Hendrix, Schrimpf, Höller, & Lamb, 2013), compared to the single-point confocal methods, because the fluorescence is collected over a larger area (typically > 64^2 pixels^2). Limitations of this technique are that the fluctuation analysis needs a certain degree of homogeneity in the sample to be performed and that RICS cannot be used to build pixel-resolution diffusion or concentration maps because the information is averaged over space.

ARICS (Arbitrary region Raster Image Correlation Spectroscopy) is a RICS improvement developed in August 2016 by Hendrix in the Lamb's group (Hendrix, Dekens, Schrimpf, & Lamb, 2016). With this particular algorithm, the regions of interest (ROIs) of any shape can be selected before starting correlation analysis, on the contrary of classical RICS. This allows to remove artefacts, to measure diffusion with subcellular resolution and to automate analysis, for example generating ROIs with shape-sensitive algorithms. The power of ARICS is the ability to create pseudo higher-resolution maps of the computed molecular parameters. In our implementation, we segmented the dataset in 16 intensity levels (ranging from the lower to the higher intensity value), that were fitted separately in order to construct diffusion pseudo-maps.

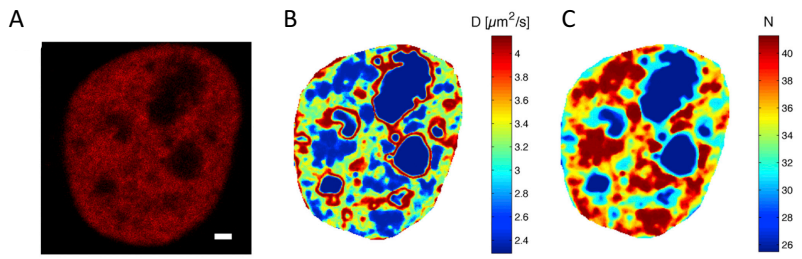

Figure 8 - ARICS Diffusion and concentration pseudo-maps.

(A) Nucleus of HeLa cells with the chromatin density fluorescent marker mRFP-H2B.
From the ARICS analysis the pseudo-diffusion map and (B) pseudo-concentration map (C) of the protein of interest, averaged over all frames.
[from: (Hendrix et al., 2016)*].*

METHODS

Animals

All experiments were carried out in accordance with the guidelines established by the European Communities Council (Directive 2010/63/EU of 22 September 2010) were permitted by the Italian Ministry of Health and followed the rules approved by the Italian Institute of Technology.

Primary neuronal cultures

Cultures of hippocampal neurons were prepared from P0-2 C57BL/6J mice of either sex. Neurons were plated at a density of $90x10^3$ cells per ml on polylysine pre-coated coverslips and kept in serum-free Neurobasal-A medium added with B27 2%, GlutMAX 1% (Invitrogen, Italy) Gentamycin (5mg/mL) at 37°C in 5% CO_2 for 16–18 DIV. Neurons were transfected at 5-7 DIV with plasmids encoded for EGFP; GABAAR-β3-phGFP; GABAAR-α1-HA; Gephyrin-EGFP or Gephyrin-Delta-2-188-EGFP using Effectene (Qiagen, Germany) following the manufacturer's protocol. Measurements were performed 5-7 days after transfection, at room temperature and keeping cells in a live cell extracellular solution. Ringer external solution contained (in mM): 145 NaCl, 5 KCl, 1 CaCl2, 2 MgCl2, 10 glucose and 10 HEPES, pH 7.4.

Cell lines cultures

HEK and N2a cells were cultured following standard protocol and grown in DMEM (Invitrogen, Italy) added with Penicillin/Streptomycin 1% and Fetal Bovin Serum 10% (Invitrogen, Italy) kept at 37°C in 5% CO_2. Cells were plated on 18mm glass coverslips and let grow overnight.
Cells lines were transiently transfected with plasmids encoding for EGFP; GABAAR-β3phGFP; GABAAR-α1HA; Gephyrin-EGFP or Gephyrin-Delta2-188-EGFP using Effectene (Qiagen, Germany) following the manufacturer's protocol. Measurements were performed 24-48 h after transfection, at room temperature and keeping cells in the aforementioned live cell extracellular solution.

Plasmid constructs

- EGFP was expressed from the pEGFP-N1 (Clontech).
- EGFP-gephyrin and mRFP-gephyrin were kindly provided by Professor E. Cherubini.
- EGFP-gephyrin 2-188 was obtained as previously described (Maas et al., 2006).
- GABA(A) receptor subunit β3SE was a gift from Tija Jacob & Stephen Moss (Addgene plasmid # 49171) (Jacob, 2005).
- Hemagglutinin (HA)-tagged a1 GABAA receptor protein was obtained by introducing an oligonucleotide encoding for HA between the IV and V residue of the mature protein in the pCDM8-a1subunit GABAAR plasmid, taking advantage of the Agilent mutagenesis kit. HA-tagged

All constructs were verified by DNA sequencing.

Antibodies and drugs

- Rat monoclonal anti-HA from Roche (1186742300, RRID: AB_10094468).
- QDot 655 goat F(ab')2 anti mouse IgG from Thermo Fisher (Q11022MP, RRID: Q11022MP).
- Dextran from Leuconostoc 40 KD from Sigma (product code: 31389).
- Casein from Vector lab (SP 5020).
- Effectene transfection kit from QIAGEN (301427).

Software for SPT analysis

Memtamorph 2016 (v. 7.8.0.0) from Molecular Devices; RRID:SCR_002368.

Matlab 2008a from Matworks.

Turbo Output 2007 (v. 16.0.0)

Excel 2017 from Microsoft Corporation.

Graph Pad Prism 2007 (v. 5.01) from Graph Pad Software.

SPT QD labelling

QD staining of surface GABAAR was performed according to previously described protocols (Petrini et al., 2009). Briefly, rat anti HA antibody was premixed with anti-mouse QD 655 (Thermo Fisher) for 25 min in the presence of casein (Vectorlab, Italy) to prevent nonspecific binding. The absence of QD labelling when the primary antibody was omitted from 'QD–antibody premix' in control experiments indicated that QD binding was ruled by the antibody specificity (data not shown). The specificity of QD labelling was demonstrated by the exclusive binding of anti-HA-coupled QDs to GABAAR α1-HA-transfected neurons, while neighbouring non-transfected

neurons were not labelled. Neurons were then incubated with the diluted antibody–QD premix for 3 min at room temperature to obtain a final QD concentration of approssimatively 0.1 nM. In the case of hybrid (FCS+SPT) experimental condition we used the QDs 10 times more concentrated to maximise the fraction of GABAAR-antibody-QD complex. Live-cell imaging and QD recording were performed by acquiring 1200 consecutive frames at 20Hz (1 min) with a 512x512 pixel EM-CCD camera (9100, Hamamatsu, Japan) using Metamorph software (ver. 7.8, Molecular Devices, USA). The highly diluted QD labelling resulted in <30 QDs per field of view, so that individual QD receptor complexes did not overlap the trajectories of neighbouring complexes. When, occasionally, two QDs were too close to unambiguously reconstruct their individual trajectories, both QDs were discarded from the analysis. During the experiments, neurons were kept at 30 °C in an open chamber filled with the recording solution. Phluorin fluorescence was acquired with 100–500ms integration time to obtain the background images. Samples were illuminated in epifluorescence with a led system (Lumencore). Phluorin and QD655 fluorescence signals were observed with appropriate excitation (435/40 and 472/30 nm, respectively) and emission filters (520/35 and 655/15 nm, respectively) (Semrock, Italy) controlled by filter wheels mounted onto an inverted microscope (Eclipse Ti, Nikon, Japan) equipped with a x60 oil 1.4 numerical aperture (NA) and x100 oil 1,4 immersion objectives.

SPT analysis

In the SPT experiments 1-min-long (1200 frames) movies were recorded at each time point to take into account the variability of the diffusive behaviour of surface receptors. The analysis was focused on QD-receptor complexes that were present in the visual field during the 1-min-long movies for their final quantification. The maximum duration of the experiment was 30 minutes. The treatment with dextran was performed by substituting the recording solution with the same extracellular solution added with dextran 40 kD (10% w/v). Control measurements were performed

adding the extracellular+dextran 10% solution from the beginning of the experiment, to check if the timing of the adding the dextran solution is relevant and no differences was detected (data not shown).

For SPT tracking, single QDs, recognized by their diffraction limited fluorescence spot shape and characteristic blinking, were followed with 50-ms time resolution. QD spatial coordinates were identified in each frame as sets of >5 connected pixels using two-dimensional object wavelet-based localization (Derkach, Oh, Guire, & Soderling, 2007) at sub-diffraction limited resolution (40 nm) with MIA software based on simulated annealing algorithm (Shiva K. Tyagarajan et al., 2013). Continuous tracking between blinks was performed with an implemented version of custom software originally written in MATLAB (The Mathworks Inc., Italy) in Dr Choquet's lab. The method is based on a QD maximal allowable displacement (5 pixels) during a maximal allowable duration of the dark period (10 frames, corresponding to 0,5 s acquisition). This stringent reconnection of trajectories across QD blinking combined with the highly diluted QD labelling have been set to avoid erroneous reconnection of neighbouring QD in the same trajectory and to provide unambiguous observations of individual receptor QD complex trajectories. Although the definition of the compartments was diffraction limited, the sub-wavelength resolution of the single particle detection (40 nm) allowed accurate description of receptor mobility within such small regions. Instantaneous diffusion coefficients, D, were calculated as previously described (Tardin, Cognet, Bats, Lounis, & Choquet, 2003b) from linear fits of the n=1–4 values of the MSD versus time plot, according to the equation: MSD(t) = $<r^2 4>$ = 4Dt for two-dimensional diffusion. MSD(t) was calculated according to the formula (1):

$$<r^2> = [\Sigma_{i=1}^{(N-n)}(X_{i+n} - X_i)^2 + (Y_{i+n} - Y_i)^2/(N-n)]dt \qquad (1)$$

Equation 1

for reconstructed trajectories of 1200 frames using a custom-made software developed by Dr Choquet (Bordeaux, France). To better characterize receptor mobility, receptor QDs have been distinguished into 'mobile' and 'immobile' populations by using as a threshold the local minimum of the bimodal distribution of synaptic GABAAR diffusion coefficients (0.0075 $\mu m^2/s$) (Tardin et al., 2003b). Next, the diffusive properties of the mobile receptor population were described as their means ± SEM. The immobile receptor population was described by the immobile fraction defined as the relative duration of the residency of a receptor QD in a given compartment with coefficient $<0.0075\ mm^2/s$.

Statistics

Values are given as means ± s.e.m. Statistical significance was tested using Graph Pad Prism 5 Software (GraphPad, USA). Normally distributed data sets were compared using the unpaired two-tailed Student's t-test, whereas non-Gaussian data sets were tested by two-tailed non-parametric Mann–Whitney U-test. In case of paired non- parametric values, Wilcoxon paired test was used. All statistical tests were two-tailed.

Indications of significance correspond to P-values < 0.05 (*), P < 0.01 (**), P < 0.001 (***) and P > 0,05 non-significant (ns).

FCS Analysis

Before FCS analysis, all the raw data were processed for afterpulse removal using a custom fluorescence lifetime correlation spectroscopy (FLCS) algorithm (Lanzanò et al., 2017).

The ACFs have been calculated for values of the correlation time *t* between 0.1 µs and 1 s.

Model for ACF analysis: The filtered ACFs have been fitted to a 3D Gaussian diffusion model:

$$G(t) = G(0)\left(1+\frac{t}{t_D}\right)^{-1}\left(1+\frac{t}{k_z t_D}\right)^{-1/2}$$

Equation 2

where G(0) is the amplitude of the ACF, kz = *wz/w* is the ratio between the size of the effective volume along z and x–y, respectively, and t_D is the characteristic transit time:

$$t_D = \frac{w^2}{4D}$$

Equation 3

In our setup, k >>1, so that we can use the approximate formula:

$$G(t) \approx G(0)\left(1+\frac{t}{t_D}\right)^{-1}$$

Equation 4

Equation 4 can be used to calibrate *w* or to determine *D*. The amplitude G(0) is inversely proportional to the number of particles N in the observation volume V:

$$G(0) = \frac{\gamma}{N}$$

Equation 5

where γ is the PSF-model dependent gamma factor(Nagy, Wu, & Berland, 2005)(γ = 0.35 for a 3D Gaussian PSF). Equation 5 is used to calculate the non-corrected number of particles N.

FCS and RICS setup

FCS measurements were performed on a custom confocal microscope described in (Vicidomini et al., 2014) equipped with a Leica 1.40 NA 100x objective (HCX PL APO 100x 1.40/0.70 Oil, Leica Microsystems). Briefly, the fluorescence light was collected by the same objective lens, de-scanned, and passed through the dichroic mirrors as well as through a fluorescence band pass filter (ET Bandpass 525/50 nm, AHF analysentechnik) before being focused (focal length 60 mm, AC254-060-A- ML, Thorlabs) into a fiber pigtailed single-photon avalanche diode (PDM Series, Micro Photon Devices, Bolzano, Italy). Photon arrival times were detected at each pixel by a time-correlated-single-photon-counting-card (TCSPC-830, Becker & Hickl). All imaging operations were automated and managed by the software Inspector (Max Planck Innovation). For the excitation light, the average power P was measured at the back aperture of the objective lens. Due to losses in the objective lens, the power at the sample is actually lower by 15% at 488.
For each cell, measurements were acquired in the cytoplasm at a distance ~2 μm above the coverglass.
Excitation power was set to 5 μW for measurement of cytoplasmic proteins and to 1 μW for measurements of membrane proteins both with a measurement duration of 30 s.

The autocorrelation function was computed by a custom-made algorithm made by Luca Lanzanò and Lorenzo Scipioni using Matlab 2016 or 2017 (Matworks). The fitting procedures both with the one component and two components models were realized with an automatic Matlab based software written by Alice Bartolozzi.

Software for FCS analysis

Matlab 2016 or 2017 form Matworks for FCS and RICS analysis.

FCS calibration

For calibration, aqueous solutions of purified EGFP (BioVision, Inc., Milpitas, CA) were prepared by diluting the protein in PBS (phosphate-buffered saline 1×, Thermo Fisher Scientific) at a final concentration of ~100 nM. For each measurement, a ~10 µl drop was deposited onto multi-well chambered cover glass previously treated for 1 h with a 1% BSA solution to prevent protein sticking to the glass. Acquisition was performed ~2 µm above the coverglass for a total acquisition time of 100.

RICS parameters

Continuous low frequency frame images were captured to compute the ARICS algorithm (Hendrix, Dekens, Schrimpf, & Lamb, 2016). Results are presented as: First frame of the stack (intensity fluorescence); diffusion coefficient (DC $\mu m^2/s$) pseudo-colour image; G_0 pseudo-colour image; Number pseudo-colour image and Brightness pseudo-colour image.

Pixel size = 20nm

Pixel dwell time = 50µs

The ACFs and fitting procedures to obtain the parameters (diffusion coefficient, G_0 number and brightness) for each pixel were performed in Matlab 2016 or 2017 (Matworks) using a home built routine (Provided by Lorenzo Scipioni).

RICS provide measurements of DC over a dynamic range of approximately 4 orders of magnitude exploiting the fact that the scanning speed along the Y direction is 2 orders of magnitude slower than the speed along the X direction.

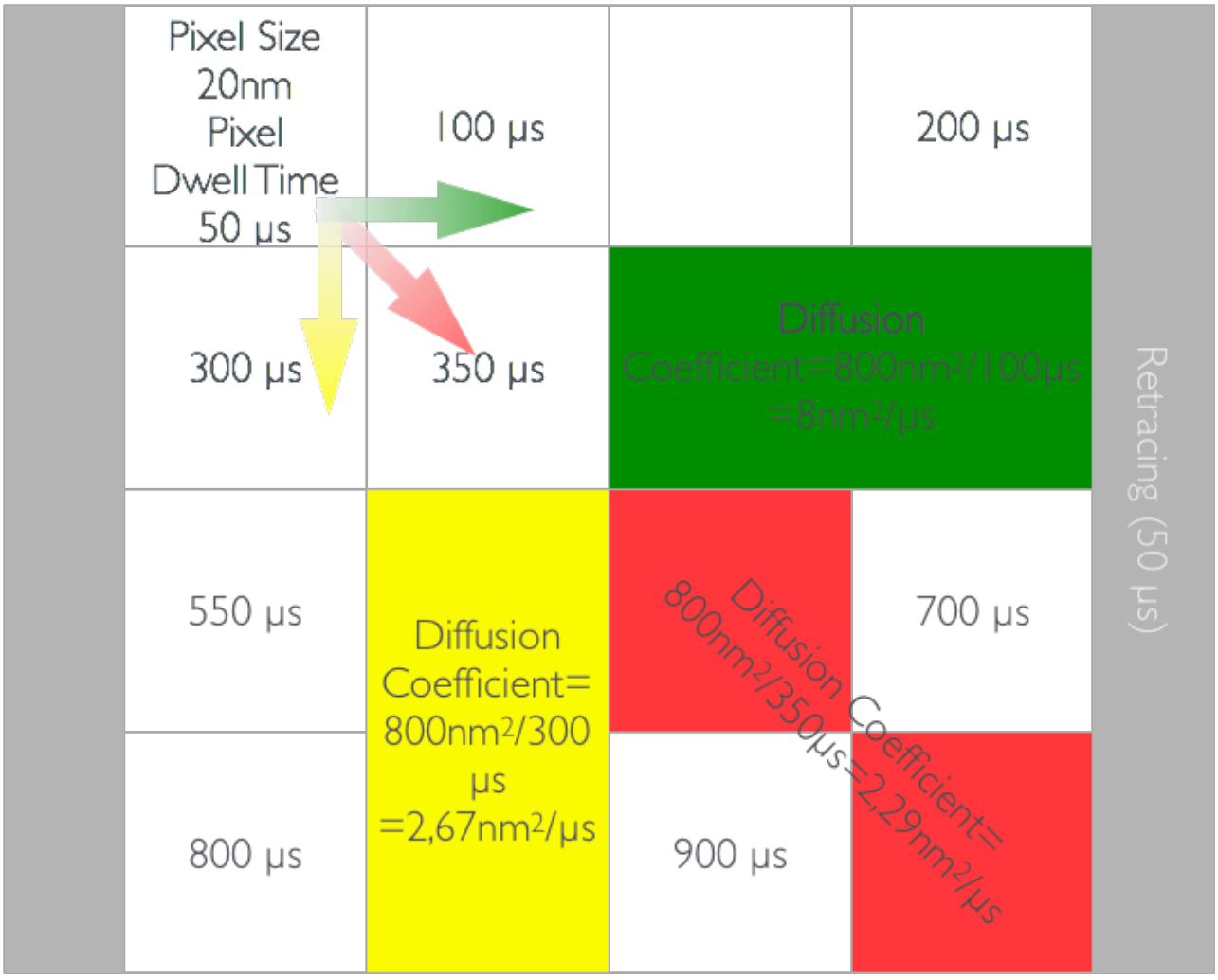

Figure 9 - RICS functioning scheme.

Each square represents a pixel (pixel size=20nm) where the slide of the confocal takes 50µs to capture the fluorescence signal (pixel dwell time=50µs). The diffusion coefficient of a fluorescent protein or molecule, is related to the length and the direction of the stripes it creates passing through the sample. The three arrows (and the three stripes) represent examples of three different molecules that take distinct times to move across the same area (2 pixlels=800nm^2).

RESULTS

The functioning of the synapse, a specialized structure that ensures the communication between neurons, relies on the tight interactions between several transmembrane and intracellular proteins at both the pre- and post-synaptic sites. At post-synaptic level, the dynamic interaction between synaptic receptors and anchoring scaffold proteins has been demonstrated to play an important role in the tuning of the synaptic strength, thus modulating neuronal activity and network activity. How protein diffusion influences synaptic plasticity by regulating the availability of synaptic receptors at synapses remains a major challenge in synaptic physiology.

In the attempt to better understand the mechanism underlying, the complex interaction among synaptic proteins at synaptic and extrasynaptic regions, we used the single point Fluorescence Correlation Spectroscopy (FCS) and the Arbitrary Raster Image Correlation Spectroscopy (ARICS), two spectroscopy approaches that allow to study the coordinated dynamics of either GABAergic receptor on the plasma membrane and gephyrin scaffold protein in the cytoplasmic space.

Gephyrin intracellular dynamics revealed by Fluorescence Correlation Spectroscopy (FCS)

FCS is an established technique to study the mobility of molecules and to measure the protein diffusion parameters with high statistics in unperturbed live cell, in both plasma membrane and cytoplasmic space.

To test the accuracy of FCS technique to measure the mobility of intracellular proteins in different compartments, in a first set of experiments, we applied FCS on heterologous systems, as simplified experimental models with respect to neurons. Initially we used Human Embryonic Kidney cells (HEK293) transfected with gephyrin fused with GFP (Figure 10).

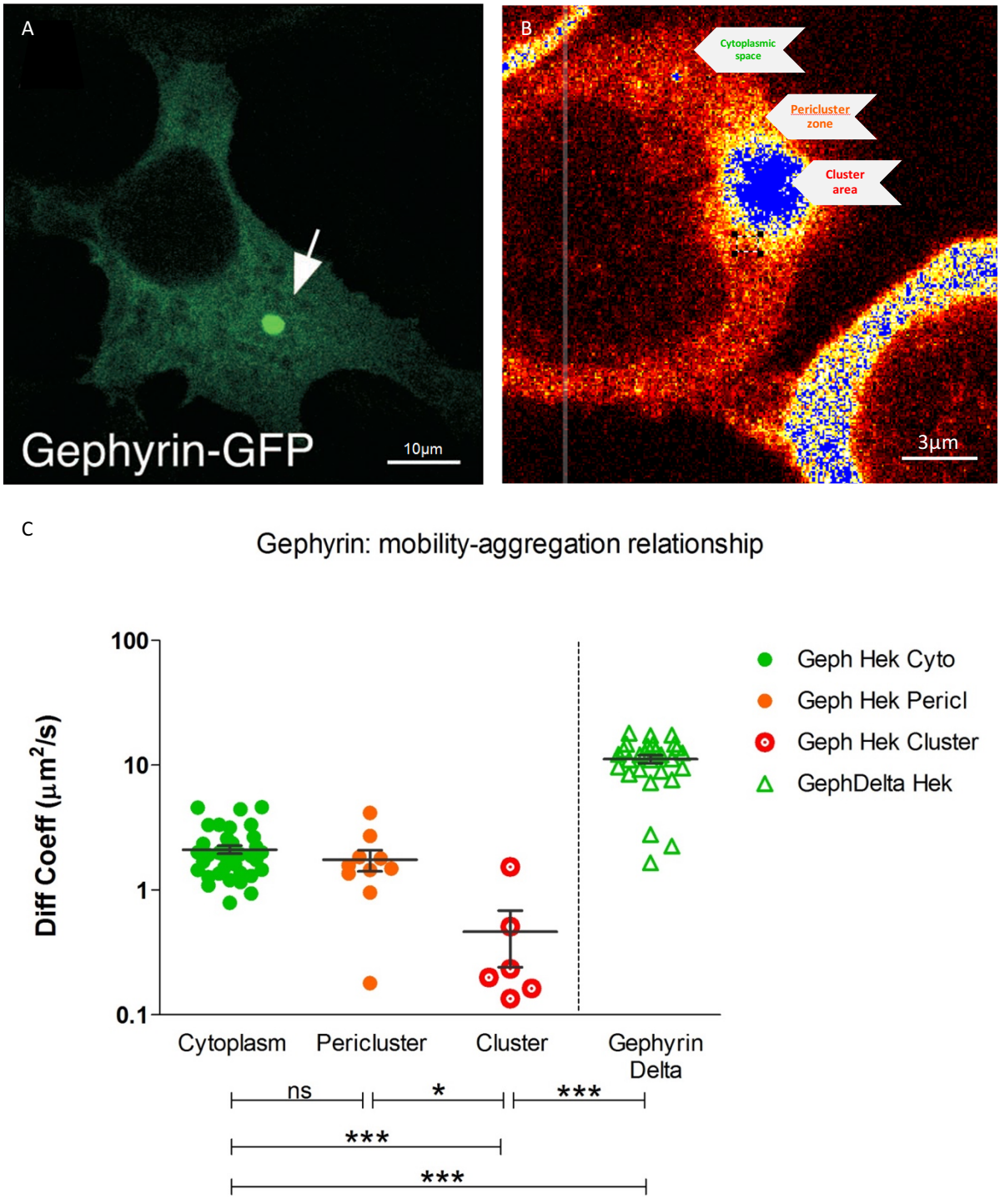

Figure 10 – Gephyrin: mobility-aggregation relationship.

Vertical dot plot of diffusion coefficient [µm2/s]. (A) Example of HEK293 cell transfected with Gephyrin-GFP with a gephyrin-GFP cluster (white arrow).
(B) Detail of a gephyrin-GFP cluster (pseudocolors). Grey arrows indicate the focus point of the FCS laser beam: in the cytoplasmic space, in the pericluster zone or cluster area. The pseudocolor scale of gephyrin-GFP intensity fluorescence goes from red (lower) to yellow (medium) to blue (higher).
(C) Average and standard error of Gephyrin-GFP in different subcellular compartments: cytoplasmic (green), pericluster (orange), cluster (red) and cytoplasmic Gephyrin-Delta-GFP (green triangles).
Indications of significance correspond to P-values < 0.05 (*), P<0.01 (**), P<0.001 (***) and P>0,05 nonsignificant (ns).

Overexpressed gephyrin-GFP displayed low fluorescence intensity, diffuse cytoplasmic localization and high intensity self-aggregating clusters that are reminiscent of synaptic cluster (Figure 10A and 10B: overexpressed gephyrin-GFP). In these conditions, we studied the biophysical properties of this protein in different aggregation states selectively focusing the FCS laser beam in the cytoplasmic space, peri-cluster zone or cluster area (Figure 10c). FCS curves were analysed with custom-made algorithms (see methods), extracting the diffusion coefficient in a large resident time range (τ_D), from $\tau_D \approx 10^{-5}$ s (correspondent to a DC$\approx 10^2$ $\mu m^2/s$) to $\tau_D \approx 10^1$ s (correspondent to a DC$\approx 10^{-4}$ $\mu m^2/s$). We identified the appropriate range between 10^{-4} and 10^0 s (DC from 10^2 to 10^{-3} $\mu m^2/s$). Then, from the autocorrelation curves of the fluorescent intensity versus time measurements, we calculated the diffusion coefficient and the concentration of the gephyrin-GFP in the three different previously mentioned subcellular compartments.

The vertical scatter plot (Figure 10c) described the gephyrin dynamics and the relationship between the diffusion coefficient and the aggregation state: low complexity of the aggregation state outside the cluster and, on the other hand, higher complexity within it.

Gephyrin-GFP freely diffused in the cytoplasmic space (Figure 10c - green dot - cytoplasmic gephyrin DC=2,10±0,16 $\mu m^2/s$ n=38 from n° cultures > 3) and the average mobility of Gephyrin-GFP only slightly decreased in the pericluster area (Figure 10c - orange dots - pericluster gephyrin DC=1,75±0,34 $\mu m^2/s$ n=10 from n° cultures > 3 || P=0,24 ns Mann-Whitney test), while being markedly reduced in the cluster core (Figure 10c - red circle – cluster gephyrin DC=0,46±0,22 $\mu m^2/s$; n=6 from n° cultures > 3 || P=0,0005 *** Mann Whitney test). Such gephyrin diffusion coefficients values likely reflect different gephyrin aggregation state in the cytoplasmic fraction with respect to those nearby or inside the cluster.

To better clarify the relationship between the aggregation state of diffusive gephyrin and the mobility, we used a mutant form of gephyrin delta 2-188 reported to impair gephyrin polymerization (Maas et al., 2006) .

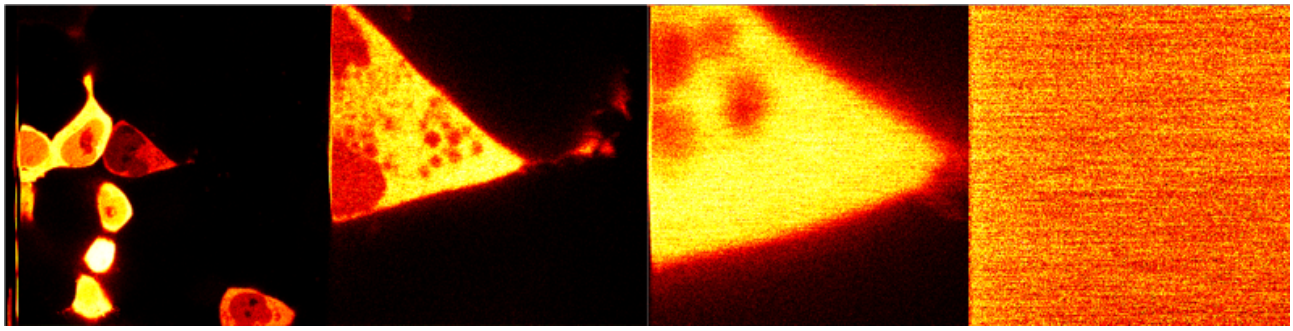

Figure 11 - Overexpressed gephyrin delta 2-188 GFP in HEK cells.

Squares dimension (from left to right) 100x100 – 20x20 – 5x5 – 1x1µm.

Based on structural investigation on the gephyrin polypeptide, the Kneussel's group generated a NH2-terminal truncated gephyrin polypeptide (amino acids 2–188) fused to EGFP. This mutant protein allows the N-terminal G trimerization motif, but lacks the C-terminal E dimerization motif of gephyrin and then represents a dominant-negative protein. Thus, this gephyrin deletion mutant interferes with the incorporation of endogenous gephyrin into a hexagonal scaffold formation (Maria Sola et al., 2004), whereby reducing gephyrin cluster stability over time. As a result, cells expressing this gephyrin mutant show the loss of endogenous gephyrin clusters, both in HEK cell then in neurons.

Also in this case, the FCS measurements were performed by focusing the laser beam in the cytoplasmic space to measure the cytosolic free diffusion of gephyrin-delta-GFP. Gephyrin delta showed dynamics significantly faster with respect to wild type gephyrin, as expected for a protein with reduced polymerization or interaction states (Figure 10c – green triangles – gephyrin delta DC=11,19±0,80 µm^2/s; n=28 from n° cultures > 3 || Gephyrin cytoplasm VS gephyrin delta P<0,0001 *** Mann Whitney test | Gephyrin pericluster VS gephyrin delta P<0,0001 *** Mann Whitney test | Gephyrin cluster VS gephyrin delta P=0,0002 *** Mann Whitney test).

Gephyrin clusters reveal two populations

The FCS curves obtained in the cytoplasm were mostly satisfactory fitted with "one component" functions demonstrating that in this cellular subzone the gephyrin diffusion is quite homogeneous. On the contrary, the FCS curves collected in the peri-cluster and cluster zones were best fitted when a second component was added to the fitting function.

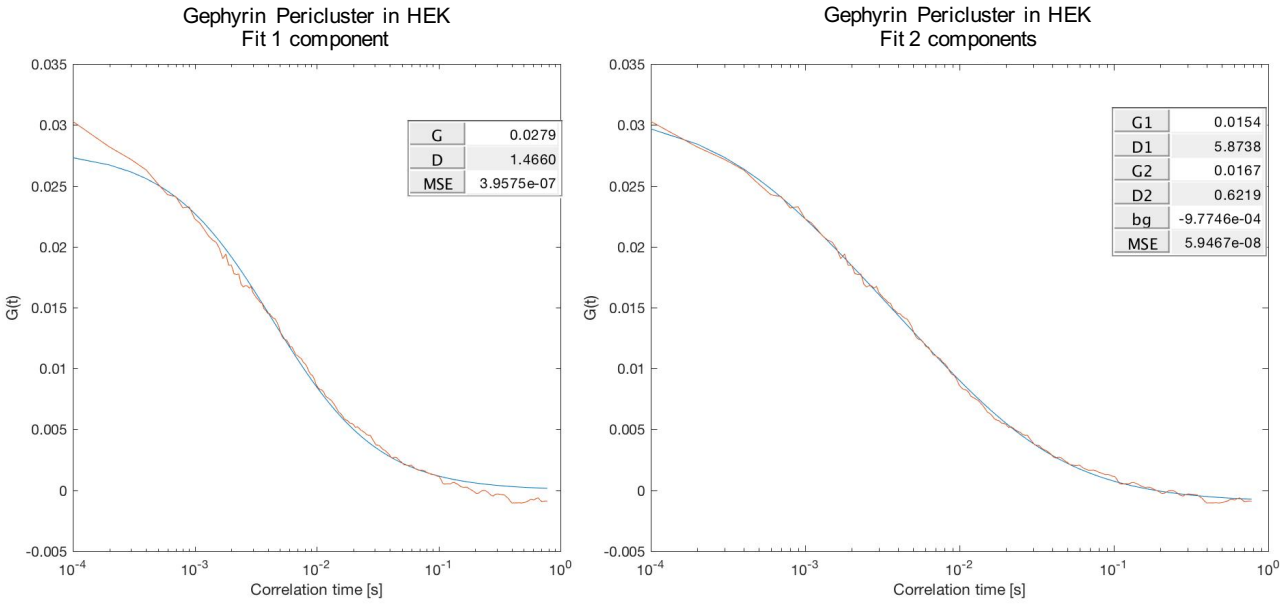

Figure 12 - Goodness of fit example.

In the two images, the autocorrelation functions (orange lines) coming from a pericluster measurements, are exactly the same, despite the fitting function models (blue lines) that admit, respectively, 1 component (left) or two component (right).
Gephyrin in the pericluster and cluster zones hides fractions revealed only with a two components model.
In this case, the slower diffusion (D2) can reflect the cluster gephyrin bounded population, in spite, the faster diffusion (D1) identifies the gephyrin mobile fraction that will establish the aggregation-removal dynamic state.

In the light of these data, we re-analysed the same pool of gephyrin FCS data by performing a two-component fit. This approach unveiled a new gephyrin diffusion coefficient component both inside the cluster and in the peri-cluster area. However, cytoplasmic gephyrin was typically satisfactory fitted with one component showing a homogenous population of fast diffusing gephyrin (cytoplasmic Gephyrin Fit1c DC=2,11±0,97μm^2/s n=38) with only few measurements displaying an autocorrelation function (ACF) better fitted with the two components (cytoplasmic Gephyrin Fit2c

D2: DC=3,79±0,83μm^2/s n=4 and D1: DC=0,10±0,04μm^2/s n=4). One population showed a diffusion coefficient similar to those coming from the previous model (one component) (cytoplasmic gephyrin VS cytoplasmic gephyrin D1 P=0,0754 ns Mann-Whitney test) and another represented a slower fraction, that differs from the previous one (cytoplasmic gephyrin vs cytoplasmic gephyrin D2 P=0,0012 ** Mann-Whitney test | cytoplasmic gephyrin D1 vs cytoplasmic gephyrin D2 P=0,0286 * Mann-Whitney test). In the pericluster zone and in the cluster areas, in contrast, almost all the measurements were better fitted with the two components function, thus demonstrating that the cluster displays "two phase dynamics". In the peri-cluster areas the two populations (D1 and D2), coming from the two component fit, showed a marked difference and both are statistically significant compared to the one component population (pericluster gephyrin Fit2c D1: DC=4,05±0,48μm^2/s n=12 and D2: DC=0,20±0,05μm^2/s n=12 || pericluster gephyrin D1 VS pericluster gephyrin D2 P<0,0001 *** Mann-Whitney test | pericluster gephyrin vs pericluster gephyrin D1 P=0,0014 ** Mann-Whitney test| pericluster gephyrin vs pericluster gephyrin D2 P=0,0004 *** Mann-Whitney test) (cluster gephyrin Fit2c D1: DC=4,41±0,96μm^2/s n=8 and D2: DC=0,06±0,03μm^2/s n=8 || cluster gephyrin D1 vs cluster gephyrin D2 P=0,0002 *** Mann-Whitney test | cluster gephyrin vs cluster gephyrin D1 P=0,0027 ** Mann-Whitney test| cluster gephyrin vs cluster gephyrin D2 P=0,0080 ** Mann-Whitney test).

We did not observe any statistically significant difference between all the faster population and between them and the one component cytoplasmic gephyrin, indicating the presence of a "free diffusion gephyrin", which is independent on the sub-region of interest (cytoplasmic gephyrin D1 VS pericluster gephyrin D1 P=0,76 ns Mann-Whitney test | cytoplasmic gephyrin D1 VS cluster gephyrin D1 P=0,46 ns Mann-Whitney test | pericluster gephyrin D1 VS cluster gephyrin D1 P=0,79 ns Mann-Whitney test). This suggests that such fast diffusion is an intrinsic property of the protein likely to be observed in any subcellular domain.

Concerning the gephyrin slow diffusion components (D2), we found more heterogeneous

dynamics, spanning almost one order of magnitude. In the peri-cluster and in the cluster areas, the D2 population slowed down ~ 10 and 100 times, respectively, with respect to the cytoplasmic gephyrin (cytoplasmic gephyrin D2 vs peri-cluster gephyrin D2 P=0,36 ns Mann-Whitney test | cytoplasmic gephyrin D2 vs cluster gephyrin D2 P=0,37 ns Mann-Whitney test | peri-cluster gephyrin D2 vs cluster gephyrin D2 P=0,034 * Mann-Whitney test).

Interestingly, inside the cluster area, the slower population of gephyrin showed diffusion values comparable to that of surface GABAA receptors calculated in the same experimental condition (Figure 13) (cluster gephyrin D2 vs GABAAR P=0,59 ns Mann-Whitney test | pericluster gephyrin D2 vs GABAAR P=0,0008 *** Mann-Whitney test). This suggested that, in the cluster compartment, gephyrin displayed a bimodal diffusion behaviour matching both the cytosolic "free diffusion" and the lateral diffusion of the GABAA receptors in the plasma membrane. The latter result supports a possible functional dynamic interaction between gephyrin and GABAA receptors. In addition, when the cytoplasmic gephyrin was found to be better fitted with two components, the cytoplasmic D2 values were in line with the GABAA receptor range diffusion (cytoplasmic gephyrin D2 vs GABAAR P=0,3395 ns Mann-Whitney test). This data suggested that the gephyrin-GABAA receptor complex could exists also outside the gephyrin cluster.

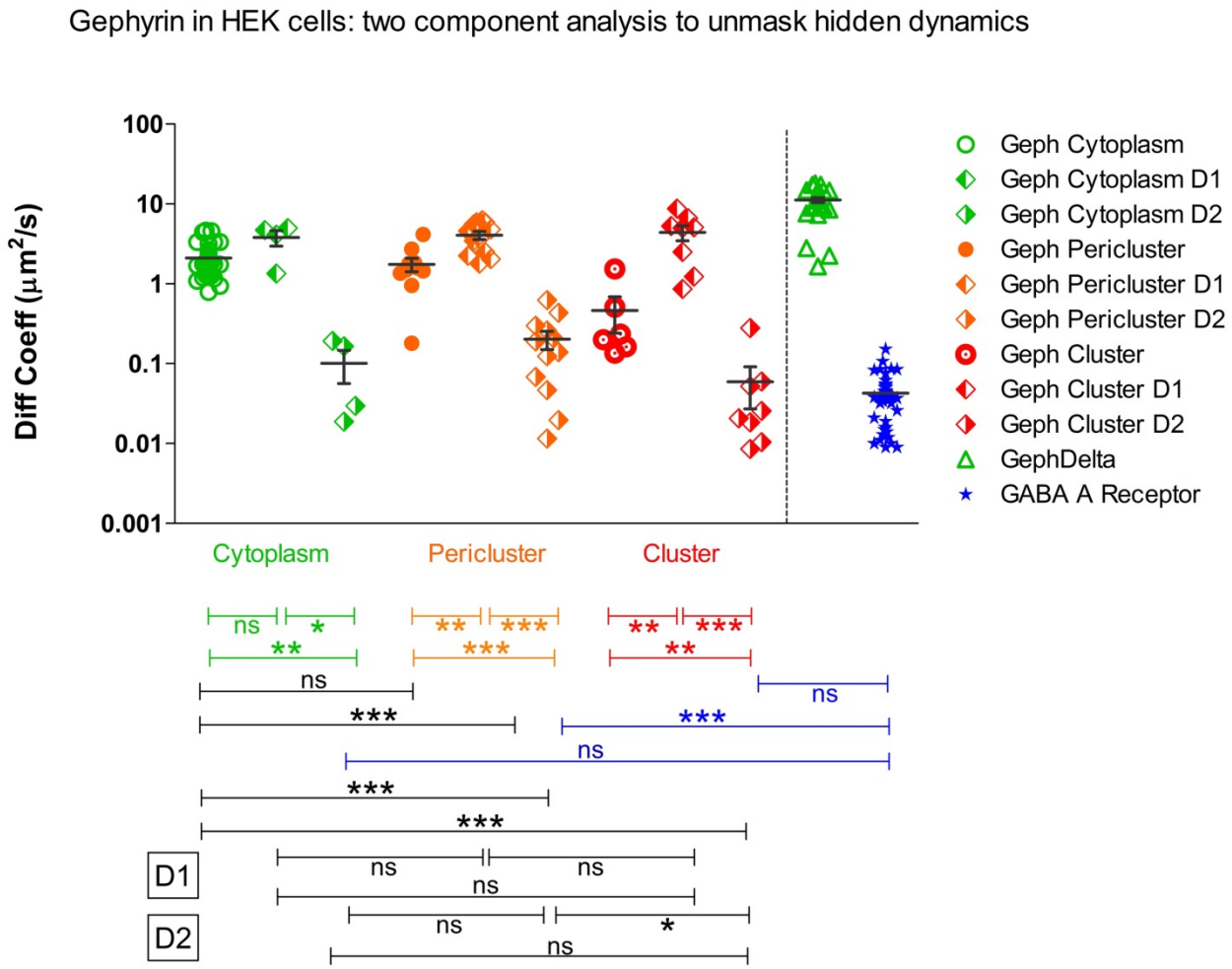

Figure 13 - Gephyrin in HEK cells to compare the values coming from the two fitting models.

Vertical dot plot of diffusion coefficient [µm2/s)
Average and standard error of Gephyrin-GFP in different subcellular compartments: cytoplasmic (one component fit green circle; two components fit green rhombuses), pericluster (one component fit orange circle; two components fit orange rhombuses), cluster (one component fit red circle; two components fit red rhombuses), cytoplasmic Gephyrin-Delta-GFP (green triangles) and membrane GABAA receptor (blue stars).
Indications of significance correspond to P-values < 0.05 (*), P<0.01 (**), P<0.001 (***) and P>0,05 nonsignificant (ns).

In line with this, our data support the emerging "aggregation-removal model" where the gephyrin cluster is formed by a continuous dynamic equilibrium of insertion and deletion of gephyrin "elementary blocks". Furthermore, we speculated that the mobility range found nearby and inside the cluster (pericluster gephyrin D2: DC=0,20±0,05µm^2/s n=12 and cluster gephyrin D2: DC=0,06±0,03µm^2/s n=8 || pericluster gephyrin D2 VS cluster gephyrin D2 P=0,034 * Mann-Whitney test) indicates that also inside the cluster gephyrin molecules may significantly unveil possible "plasticity dynamics" also inside the aggregate states. This consideration supports the

cluster rearrangement in higher density nanodomains (Pennacchietti et al., 2017) related with post-synaptic synaptic plasticity.

Gephyrin "free diffusion" is cell types partially dependent: interactions or environment dependence?

In order to assess whether the gephyrin diffusion data shown in HEK cells are cell type dependent, we repeated the same experiments in Neuro2a cells (N2a), a fast-growing neuroblastoma cell line that shares some features with neurons, such as the presence of neurofilaments that are reminiscent on dendritic arborisation. To further validate our data a set of experiments were also performed in cultured hippocampal neurons (Neu). N2a and hippocampal neurons were transfected both with gephyrin-GFP and with gephyrin-delta-GFP.

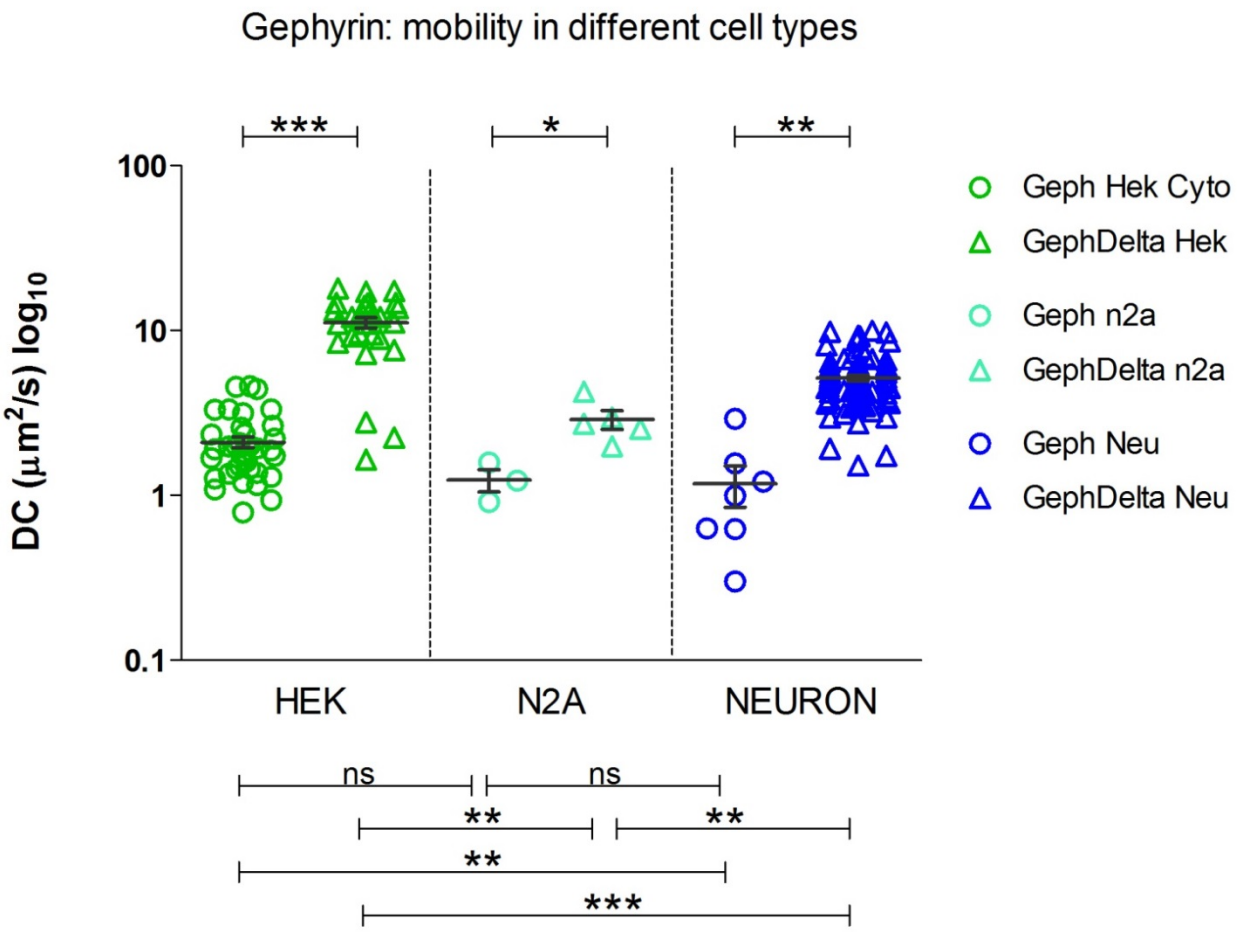

Figure 14 - Gephyrin and gephyrin delta are cell types partially dependent.

Vertical dot plot of diffusion coefficient [µm2/s)
Average and standard error of Gephyrin-GFP in different cell types:
Cytoplasmic Gephyrin in HEK cells (green circles), cytoplasmic Gephyrin-Delta-GFP in HEK cells (green triangles).
Cytoplasmic gephyrin in N2A cells (light blue circles), cytoplasmic Gephyrin-Delta-GFP in N2A cells (light blue triangles).
Cytoplasmic gephyrin in Neurons cells (blue circles), cytoplasmic Gephyrin-Delta-GFP in Neurons cells (blue triangles).
Indications of significance correspond to P-values < 0.05 (*), P<0.01 (**), P<0.001 (***) and P>0,05 nonsignificant (ns).

Then the diffusion coefficients of these proteins in the cytoplasm of both n2a and neurons were measured with the aforementioned single point FCS technique. We observed a statistically significant increase of gephyrin-delta-GFP diffusion coefficient in every cell types (Gephyrin in HEK DC=2,11±0,16µm^2/s; n=38 from n cultures>3 VS Gephyrin Delta in HEK DC=11,2±0,80µm2/s; n=28 from n cultures>3 | P<0,0001 *** Mann Whitney test | Gephyrin in n2a DC=1,25±0,0,19µm2/s; n=3 VS Gephyrin Delta in n2a DC=2,90±0,38µm2/s; n=5 from n cultures>3; P=0,04 * Mann Whitney test | Gephyrin in neu DC=1,18±0,33µm2/s; n=7 from n

cultures>3 VS Gephyrin Delta in neu DC=5,16±0,33µm2/s; n=83 from n cultures>3; P=0,0014 ** Mann Whitney test). The diffusion coefficient average of wild type gephyrin is always at least two times higher than the mutant gephyrin, suggesting that the impossibility to undergo to high level of clusterization could have a crucial role in the mobility behaviour of the protein. It is important to notice that the mobility of wild type gephyrin is quite stable across the cell lines in spite of different cellular environments. The gephyrin-delta-GFP behaves in a different manner, that is strongly influenced by the cellular environment, but also in this case the diffusion coefficient in neurons is reduced by half respect to the HEK cells (Gephyrin Delta in HEK DC=11,2±0,80µm2/s; n=28 from n cultures>3 VS Gephyrin Delta in neurons DC=5,16±0,33µm2/s; n=83 from n cultures>3; P<0,0001 *** Mann Whitney test).

Taking together, these evidences show that in hippocampal neurons the mobility of these cytosolic proteins is lower than in cell lines. Although the mobility of cytoplasmic proteins such as gephyrin and gephyrin-delta should be governed by the same diffusion laws in cells that share similar intracellular environments, the observation of suppressed diffusion in neurons is somewhat surprising. However, the reasons of this strong slowdown could be, at first sight, assigned to higher molecular intracellular density or binding interactions.

EGFP diffusion decreased in neurons: molecular crowding or volume confinement drive the intracellular translational mobility

To explore the hypothesis that the observed reduction of gephyrin diffusion in neurons could be due to "crowded" intracellular environment, we used the single point FCS approach to measure the mobility of untagged monomeric enhanced green fluorescent protein (EGFP) as "reference protein" showing no specific molecular interactions (Hinde, Cardarelli, Digman, & Gratton, 2010). Overexpressed EGFP showed a homogeneous diffusion coefficient in cell lines but, interestingly, similarly to gephyrin, the EGFP mobility was significantly reduced in hippocampal neurons(Figure

15) (EGFP in HEK DC=32,17±2,27µm2/s; n=11 from n cultures>3 | EGFP in n2a DC=26,12±2,67µm2/s; n=12 from n cultures>3 | EGFP in neurons DC=11,00±0,99µm2/s; n=15 from n cultures>3 || EGFP in HEK VS n2a P=0,15 ns Mann Whitney test | EGFP in n2a VS neurons P=0,0005 *** Mann Whitney test | EGFP in HEK VS neurons P<0,0001 *** Mann Whitney test).

The EGFP diffusion coefficient values, indeed, showed almost a threefold reduction in neurons with respect to cell lines

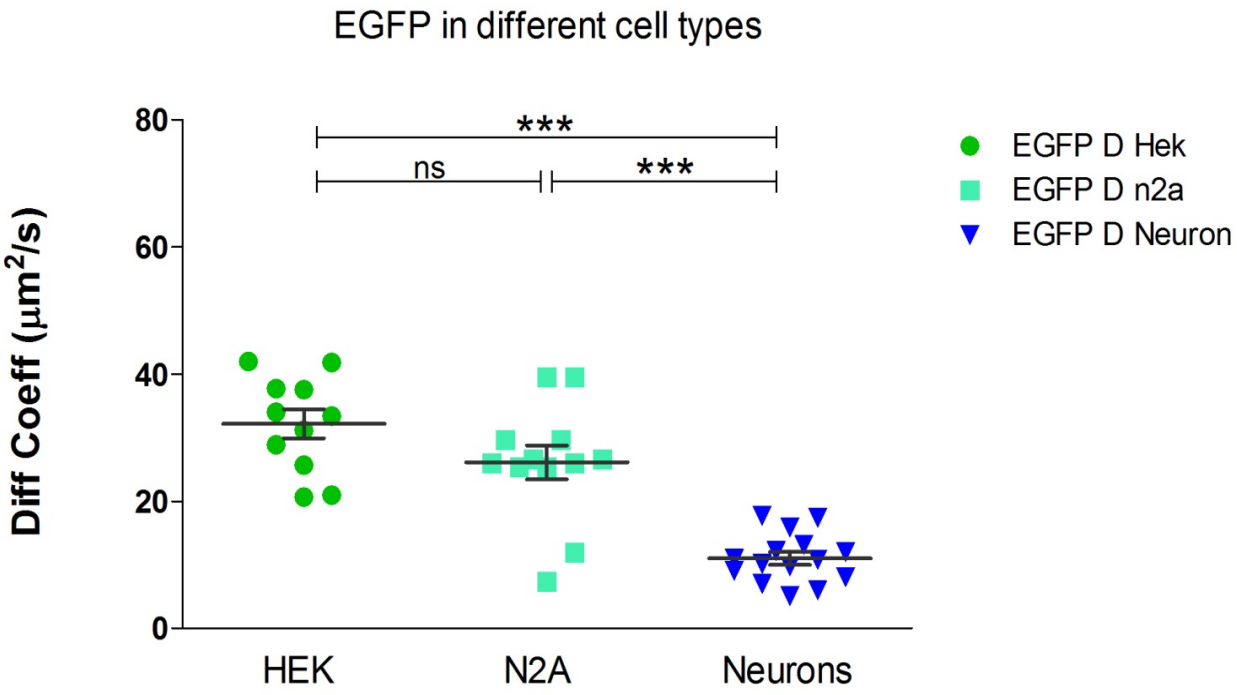

Figure 15 – EGFP slows down in neurons: molecular crowding or volume confinement.

Vertical dot plot of diffusion coefficient [µm2/s)
Average and standard error of Monomeric GFP in different cell types: monomeric GFP in HEK cells (green circles), monomeric-GFP in N2A cells (light blue square), monomeric-GFP in Neurons (blue triangles).
Indications of significance correspond to P-values < 0.05 (*), P<0.01 (**), P<0.001 (***) and P>0,05 nonsignificant (ns).

In summary, we found that the intracellular molecular diffusion strongly depends on the biophysical property of the cytoplasmic space of the cell types, including molecular crowding and/or specific cell shape/geometry.

Synaptic protein dynamics studied with Arbitrary Region Raster Image Correlation Spectroscopy (ARICS)

The ability of RICS technique to extract information on the protein mobility from fluorescence images represents an excellent tool to study the diffusion in biological samples. Since RICS is normally performed in large square image regions (typically > 64^2 pixel^2), the spatial resolution is considerably lowered when molecular parameters (diffusion, concentration, brightness, stoichiometry, and interactions) are mapped. Although ARICS allows analysis in ROIs that do not strictly need to be square, a considerable number of pixels is still needed to create a single correlation function. This leads to a similar resolution limit when mapping with ARICS. By exploiting particular image features, the ARICS method can also be used to build pseudo higher-resolution maps of molecular parameters (Hendrix, Dekens, Schrimpf, & Lamb, 2016). RICS has the advantage that the excitation energy is distributed over a much larger region in the sample. Hence, RICS and other imaging methods typically suffer much less from photobleaching-related artefacts (Hendrix, Schrimpf, Höller, & Lamb, 2013).

The slide of the confocal microscope scans the sample with a fixed speed and when the diffusion coefficient of the fluorescent molecules is in the same displacement range, stochastically, some of them will move together with the slide, drawing "strips" that once processed with the ARICS algorithm, allow to compute the diffusion coefficient and the concentrations of specific molecules of interest for each pixel of the image.

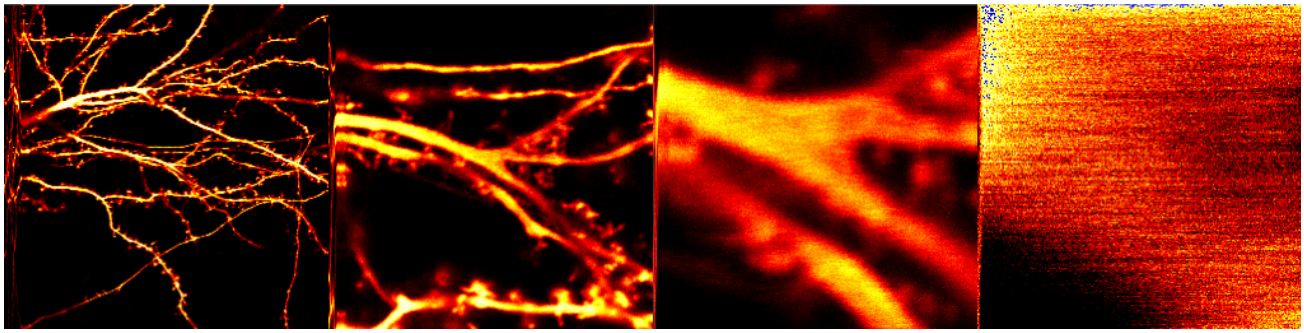

Figure 16 – Fluorescent stripes hidden in the images coming from the scanning confocal microscope.

During the whole time in which the moving species and the slide of the confocal microscope are moving together, the same amount of photons will reach the PMT producing stripes on the image.
The images sizes are (from left to right) size: 100x100 – 20x20 – 5x5 – 1x1µm.

Our algorithm identifies zones with the similar intensity and by computing the autocorrelation function provides diffusion coefficient of the fluorescent probe rendered in "pseudo-colour diffusion maps".

In the present work, we used the ARICS approach to better understand the dynamics of the cytosolic synaptic proteins. To this end, the same FCS set of experiments was performed with the ARICS approach.

We started from the monomeric EGFP transfected in the three different cell culture: HEK cells, N2A cells and neurons (Figure 17).

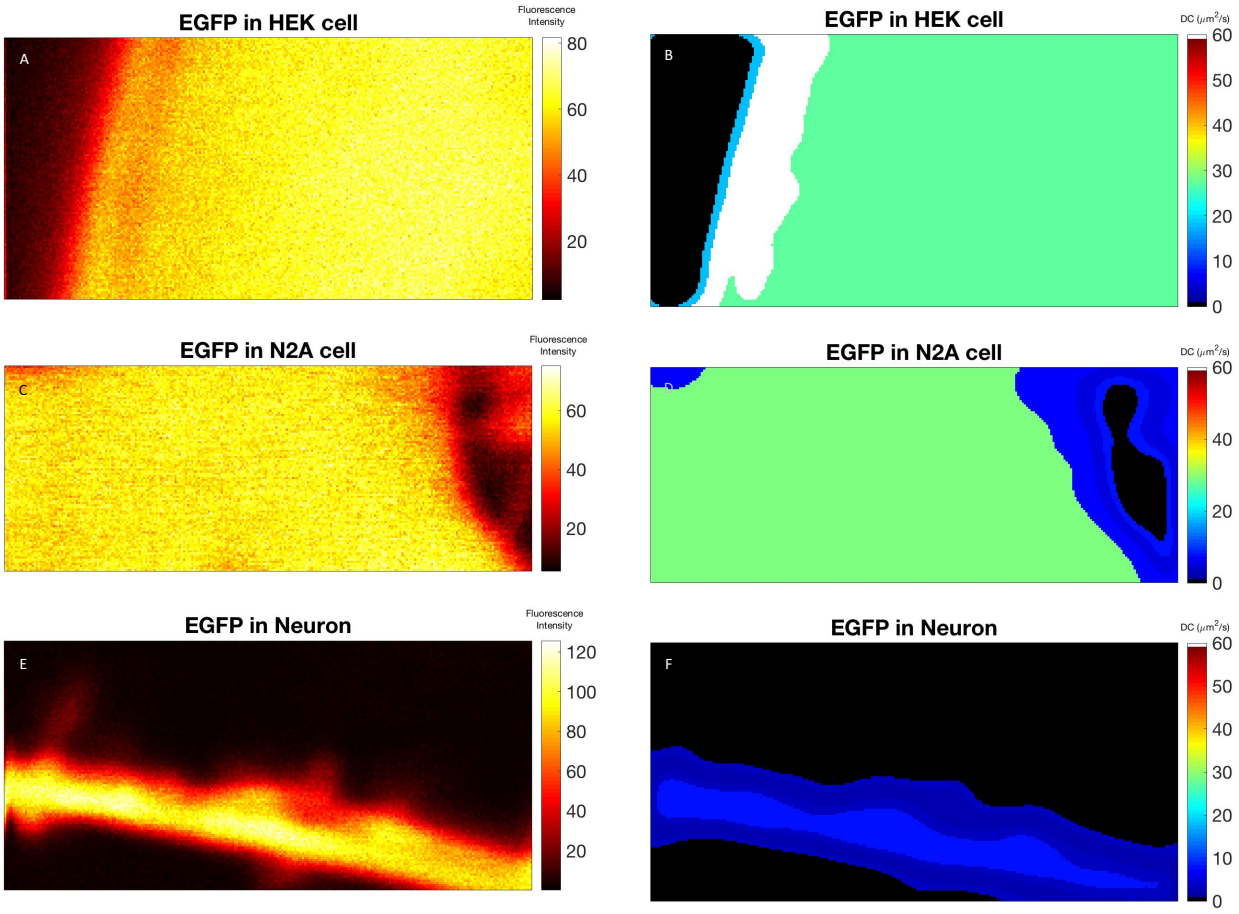

Figure 17 - EGFP dynamics measured by ARICS algorithm in the three different cell types.

EGFP in HEK cell (upper panels), EGFP in N2A cell (mid panels) and EGFP in neuron (lower panels).
(A) Example of one frame of the stack of EGFP in HEK cell; (B) ARICS pseudo-diffusion map of the EGFP in HEK cell.
(C) Example of one frame of the stack of EGFP in N2A cell; (D) ARICS pseudo-diffusion map of the EGFP in N2A cell.
(E) Example of one frame of the stack of EGFP in neuron; (F) ARICS pseudo-diffusion map of the EGFP in neuron. In the white regions, the ARICS algorithm is not able to compute the DC, instead in the fluorescence out of focus zones the DCs computed are not accurate.
All the images have the same size: 5,12x2,56 μm.

The ARICS pseudo colour-maps confirm the data previously found in the FCS experiments. The EGFP behaviour is extremely homogeneous in the whole cytoplasmic space with DC values concentrated around 30μm^2/s in each cell lines (HEK and N2A), although neurons display a slowdown of the monomeric EGFP DC to 10μm^2/s (Figure 17). In the periphery of the cell there is always a mild slowdown that could be due to the physical interaction with the cell membrane, to the smaller volume and/or to the higher crowding level in that region.

Then we transfected gephyrin-GFP in HEK cells to measure the diffusion coefficient of this protein simultaneously in the whole cell. In this case the ACFs needed a two components analysis to be correctly fitted, giving rise to two distinct pseudo-diffusion maps (D1 and D2) for each measurement (Figure 18).

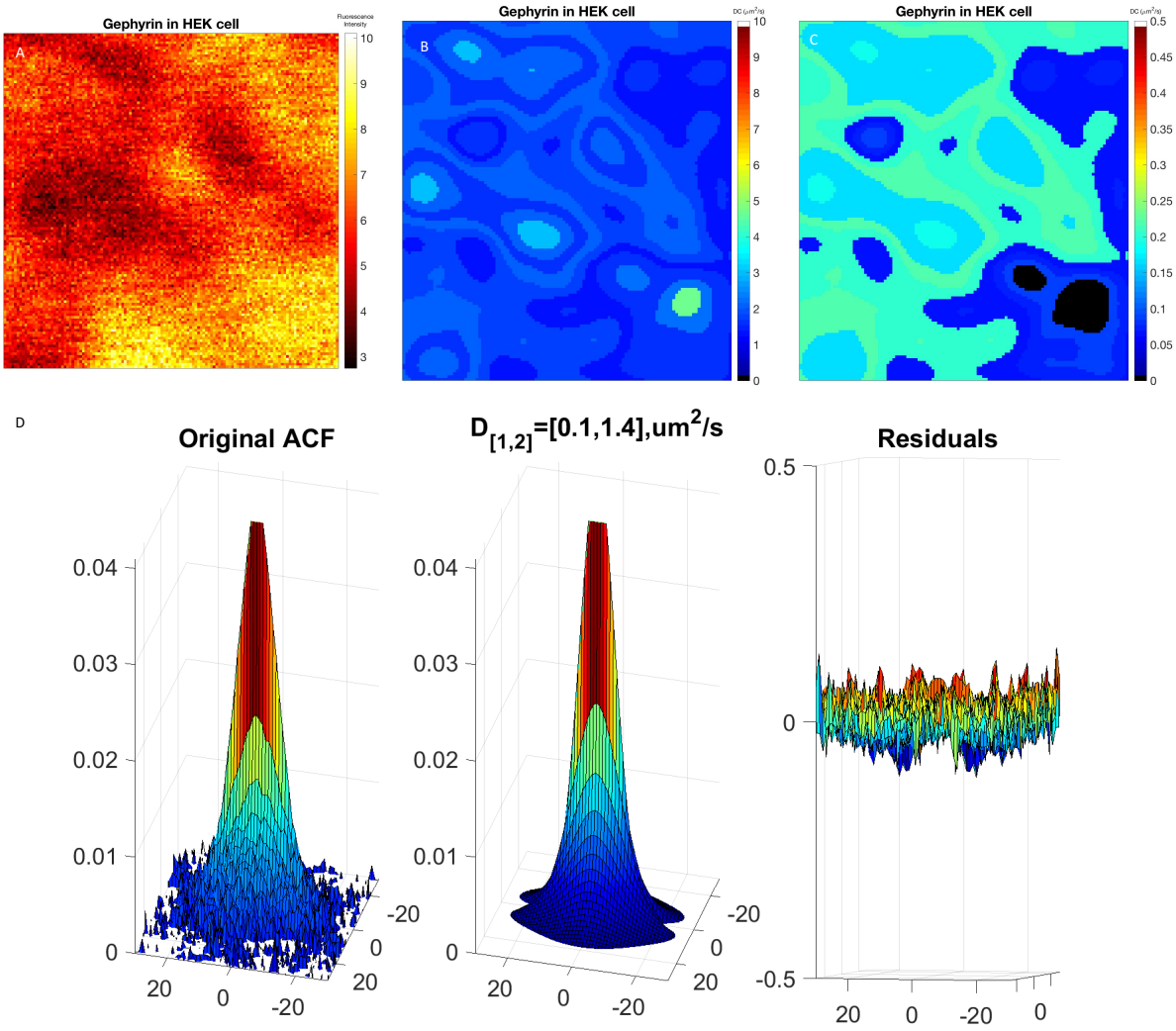

Figure 18 – Gephyrin-GFP dynamics measured by ARICS algorithm and example of fit for one general classes.

(A) Example of one frame of the stack of gephyrin-GFP in HEK cell; (B-C) ARICS Pseudo-diffusion map of the gephyrin-GFP in HEK cell coming from the two components fit: (B) diffusion coefficient D1 and (C) diffusion coefficient D2. In proximity of gephyrin-GFP high concentration areas the DC is lower, probably due to the higher concentration protein or higher clusterization levels. In the black zones the concentration is too high to be calculated by the ARICS algorithm.
(D) Autocorrelation Function (ACF), two components fit and residuals for a general class of gephyrin-GFP.
All the images have the same size: 5,12x5,12µm.

The pseudo-colour maps show a clear inhomogeneous DC along the cytoplasm, reflecting its capacity to undergo through different polymerization states in different zones. Both the fast (D1) and slow (D2) sets of DCs are in line with them measured with FCS approach. In fact, the D1 diffusion coefficients display values from 1 to 5 $\mu m^2/s$ while, the slower DCs (D2) span from 0,05 to 0,3 $\mu m^2/s$ (Figure 18).

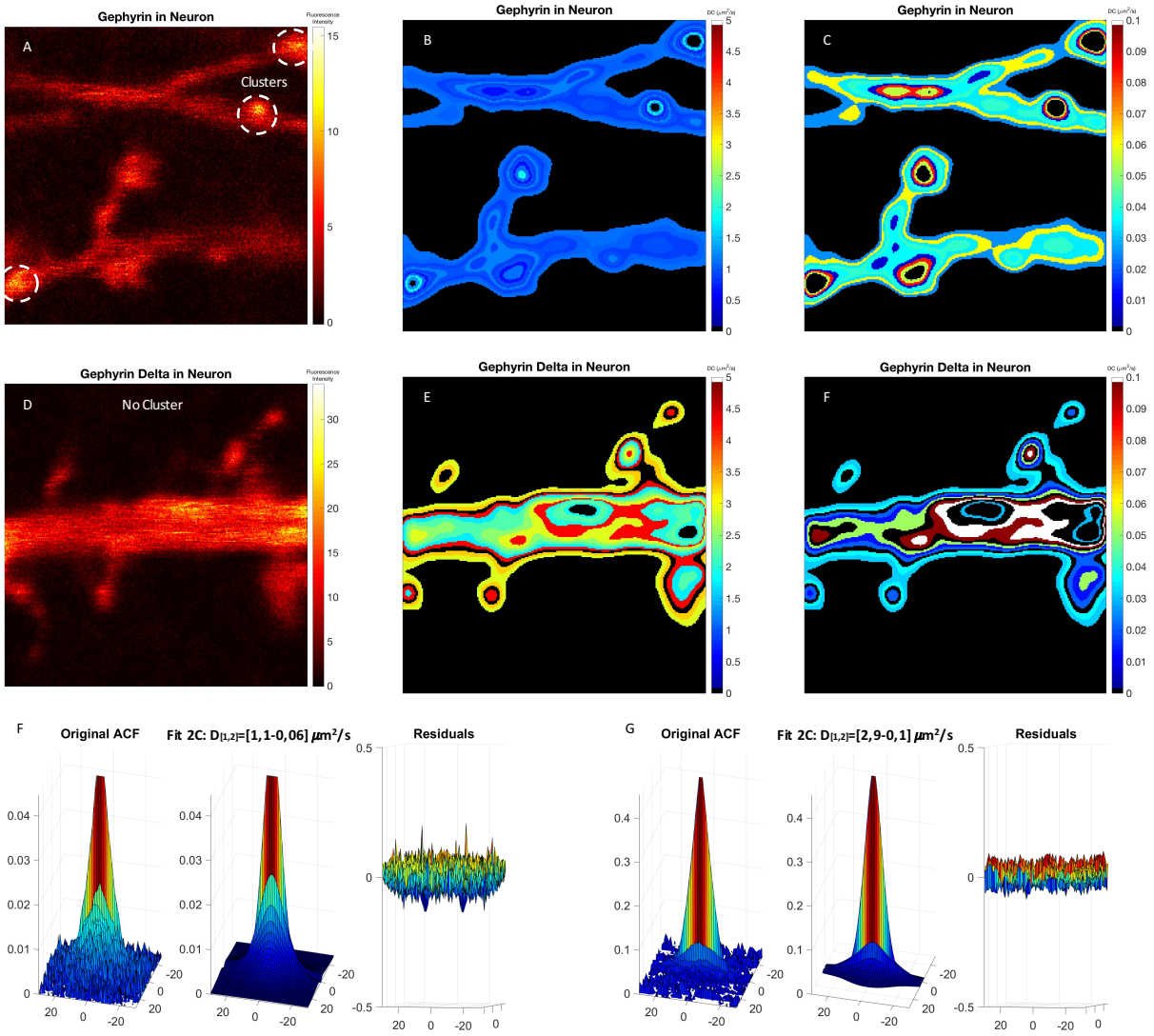

Figure 19 – Gephyrin-GFP and Gephyrin-Delta-GFP dynamics measured by ARICS algorithm and examples of fit for two general classes.

Gephyrin-GFP (upper panels), Gephyrin-Delta-GFP (mid panels) dynamics measured by ARICS algorithm and examples of fit for two general classes (lower panels).
(A) Example of one frame of the stack of gephyrin-GFP in neuron; (B-C) ARICS Pseudo-diffusion map of the gephyrin-GFP in neuron coming from the two components fit: (B) diffusion coefficient D1 and (C) diffusion coefficient D2.
Neighbouring the clusters of gephyrin-GFP (white dashed circles) there is a characteristic stratification of DC. Inside the clusters the diffusion is too slow and the concentration too high to be calculated by the ARICS algorithm.
(D) Example of one frame of the stack of gephyrin-delta-GFP in neuron.
(E-F) ARICS Pseudo-diffusion map of the gephyrin-delta-GFP in neuron coming from the two components fit: (E) diffusion coefficient

D1 and (F) diffusion coefficient D2. The gephyrin-delta-GFP shows a diffuse behaviour without the characteristic gephyrin clusters. In the black zones the concentration is too high to be calculated by the ARICS algorithm.
(F-G) Autocorrelation Function (ACF), two components fit and residuals for two general classes respectively of gephyrin-GFP (F) and gephyrin-delta-GFP (G).
All the images have the same size: 5,12x5,12µm.

The results obtained with the ARICS approach confirmed the higher mobility of gephyrin-delta-GFP respect to the WT protein (Figure 19). Furthermore, the analysis of the diffusion maps represents a new possibility to study the spatial distribution of these proteins and in particular the relationship between the concentration and the mobility of the proteins in the same areas. All the gephyrin-GFP clusters (white dashed spots) were surrounded by a characteristic area where the DC indicates that the circumference neighbouring a cluster is strictly regulated. A very interesting observation is the prevalence of the delta-gephyrin and WT gephyrin at low diffusion rate (D2) right below the plasma membrane, in the cellular sub-region where they are expected to bridge the receptors with the cytoskeleton. In particular, in these zones the DC is in the same range of the GABAA receptor DC, suggesting their mobility may be correlated. Comparing the D1 gephyrin and gephyrin-delta to the D2 pseudo-colour maps, it is possible to notice that the D2 gephyrin WT DCs at the edge are noticeably lower than the DCs in the cytoplasmic space, supporting the hypothesis of an interaction of gephyrin with membrane or sub-membrane proteins rather than a passive reduction due to the spatial constraint imposed by the membrane.

Quantify lateral mobility of GABAA receptors in neurons: comparison between current optical techniques (FCS – SPT)

Here we exploited two cutting edge techniques, FCS and SPT, to measure the lateral diffusion on the cellular membrane of the GABAA receptor (GABAAR), the main receptor mediating inhibition in the CNS.

We focused on GABAAR fused with phluorin, a pH sensitive protein that is fluorescent only when it is exposed to nearly neutral pH (on the cell surface), while it is quenched when endocytosed in the acidic intracellular vesicles.

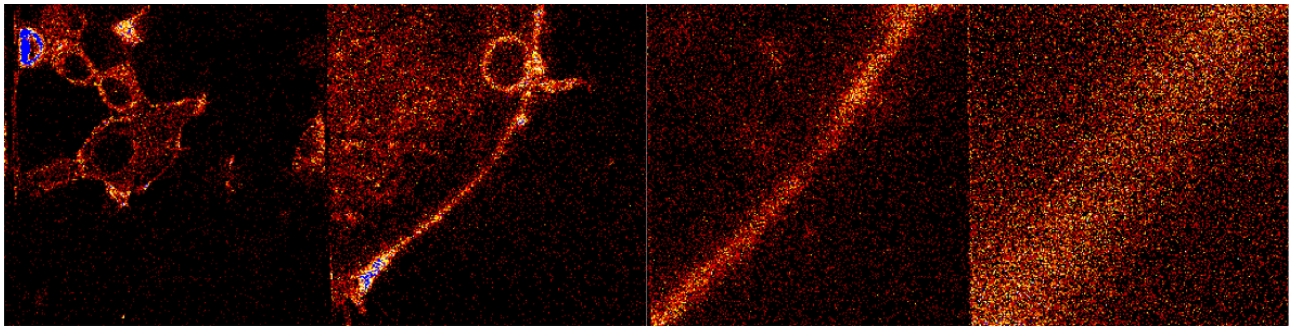

Figure 20 - HEK cells transfected with GABAAR fused with Phluorin (pH sensitive protein brightly fluorescent only on the surface). The images sizes are (from left to right) size: 100x100 – 20x20 – 5x5 – 1x1µm.

To assess the reliability of our SPT and FCS techniques we measured the diffusion of GABAA receptor a1-HA (hemagglutinin tag derived from the human influenza virus HA protein, extensively used as a general antibody epitope tag) and b3-phluorin heteromers. Interestingly, the diffusion coefficient obtained with FCS autocorrelation function are in line with those calculated with Quantum Dot based Single Particle Tracking Technique (QD-SPT) (Figure 21) (GABAAR NEU RINGER (FCS) DC=0,032±0,007µm2/s; n=17 from n cultures>3 | GABAAR NEU RINGER (SPT) DC=0,024±0,004µm2/s; n=14 from n cultures>3 || GABAAR NEU RINGER (FCS) VS GABAAR NEU RINGER (SPT) P=0,98 ns Mann Whitney test). This evidence indicates that the

Antibody+QD complex does not significantly interfere with the lateral mobility of receptors in basal condition (ringer solution) (Figure 21).

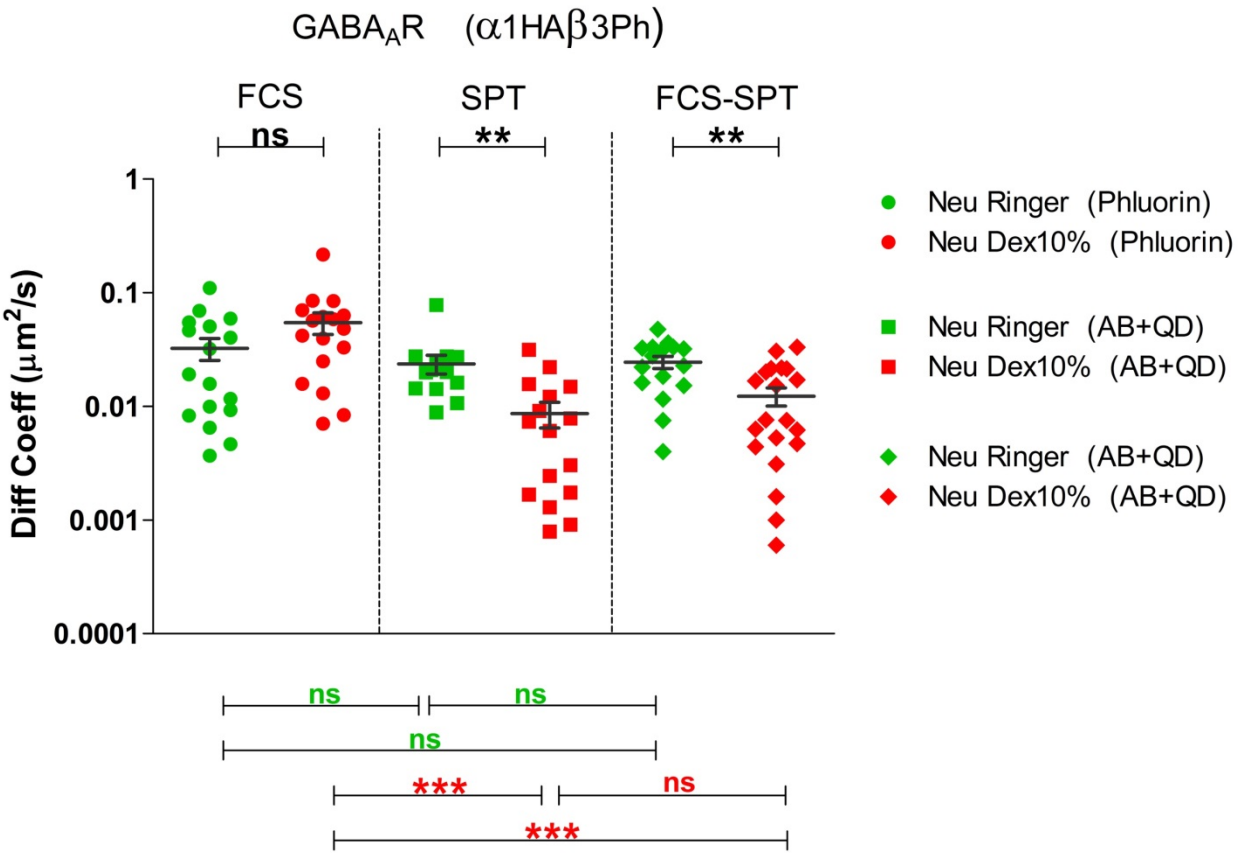

Figure 21 – GABAAR diffusion calculated with SPT and FCS display comparable values. Dextran differentially slow down only the receptors bound to the AB+QD structure.

Indications of significance correspond to P-values < 0.05 (*), P<0.01 (**), P<0.001 (***) and P>0,05 nonsignificant (ns).

In order to interfere with the receptor diffusion, we added to the extracellular solution dextran 40kD (Dex10% weight/volume), a complex branched glucan that increases the viscosity of the extracellular fluid with negligible effects on the cell metabolism (Barberis, Petrini, & Cherubini, 2004; Perrais & Ropert, 2000). Our data demonstrated that dextran slowed down the lateral diffusion of GABAA receptors in SPT experiments, while in contrast it did not interfere with the receptor diffusion probed using the FCS technique by exploiting the phluorin fluorescence (GABAAR NEU DEX10% (FCS) DC=0,054±0,012μm2/s; n=17 from n cultures>3 | GABAAR

NEU DEX10% (SPT) DC=0,009±0,002µm2/s; n=16 from n cultures>3 || GABAAR NEU DEX10% (FCS) VS GABAAR NEU DEX10% (SPT) P<0,0001 *** Mann Whitney test).

To test the hypothesis that such difference in dextran effect on GABAAR surface mobility was due to the tethering of the antibody and quantum dot (AB+QD) used in SPT we repeated FCS with the addition of AB+QD (see SPT method) with the goal to perform FCS measurements in the same experimental conditions as in SPT.

The diffusion of GABAAR bound to the AB+QD structure was measured by standard FCS phluorin intensity fluorescence. To avoid the crosstalk between the two detections systems we excluded the photons coming from the QD choosing QD655 that had a fluorescence emission far from the emission peak of the Phluorin (QD655 excitation peak ≈380; emission peak ≈655 | Phluorin excitation peak ≈488; Emission peak ≈520nm). Interestingly, the results obtained supported the hypothesis that the AB+QD complex interfere with receptor diffusion in conditions of increased viscosity of the extracellular milieau. In fact, the "hybrid" measurements (FCS technique in the presence of AB+QD complex) showed similar results to the SPT data, in which the mobility of GABAA receptor in basal condition (ringer FCS+SPT) was not impaired. However, in contrast, the application of the dextran 10% higher density solution clearly reduced the mobility of GABAA receptors (GABAAR NEU RINGER (FCS-SPT) DC=0,024±0,003µm2/s; n=16 from n cultures>3 | GABAAR NEU DEX10% (FCS-SPT) DC=0,013±0,003µm2/s; n=20 from n cultures>3 || GABAAR NEU RINGER (FCS+SPT) VS GABAAR NEU DEX10% (FCS+SPT) P=0,0040 ** Mann Whitney test).

The mobility of the GABAA receptor are rather stable across all the control experiments (ringer condition) (GABAAR NEU RINGER (FCS) DC=0,032±0,007µm2/s; n=17 from n cultures>3 | GABAAR NEU RINGER (SPT) DC=0,024±0,004µm2/s; n=14 from n cultures>3 | GABAAR NEU RINGER (FCS-SPT) DC=0,024±0,003µm2/s; n=16 from n cultures>3 || GABAAR NEU RINGER (FCS) VS GABAAR NEU RINGER (SPT) P=0,9842 ns Mann Whitney test | GABAAR NEU RINGER (FCS) VS GABAAR NEU RINGER (FCS-SPT) P=0,8712 ns Mann

Whitney test | GABAAR NEU RINGER (SPT) VS GABAAR NEU RINGER (FCS-SPT) P=0,2891 ns Mann Whitney test) indicating that the two techniques are suitable for the measure of proteins diffusing on the plasma membrane. Nevertheless, the influence of the dextran on the dynamics of the protein reflects the susceptibility of the system to the environment. Our data demonstrate the significant impact that the AB+QD structure can exert on receptor lateral mobility (Figure 21) thus raising the point that extracellular domains of transmembrane proteins may hinder the protein diffusion especially in conditions of high extracellular viscosity that are expected to take place in *ex vivo* brain slices or in *in vivo* environment due to the presence of the extracellular matrix (GABAAR NEU DEX10% (FCS) DC=0,054±0,012µm2/s; n=17 from n°cultures>3 | GABAAR NEU DEX10% (SPT) DC=0,009±0,002µm2/s; n=16 from n°cultures>3 | GABAAR NEU DEX10% (FCS-SPT) DC=0,013±0,003µm2/s; n=20 from n°cultures>3 || GABAAR NEU DEX10% (FCS) VS GABAAR NEU DEX10% (SPT) P<0,0001 *** Mann Whitney test | GABAAR NEU DEX10% (FCS) VS GABAAR NEU DEX10% (FCS-SPT) P<0,0001 *** Mann Whitney test || GABAAR NEU DEX10% (SPT) VS GABAAR NEU DEX10% (FCS-SPT) P=0,272 ns Mann Whitney test).

DISCUSSION

The present work provides the basis for the application of different spectroscopic techniques for the study of synaptic dynamics with unprecedented resolution in space and time.

The mobility of proteins at the synapse is a crucial determinant of synaptic activity. In the last twenty years, it has been demonstrated that the fast receptor exchange between synaptic and extrasynaptic sites, it is crucial for the fast tuning of the receptors number, which modulates the synaptic strength. At the level of the glutamatergic synaptic membrane, the lateral diffusion of AMPA receptors between extrasynaptic and synaptic areas modulates synaptic excitatory currents, affecting the fidelity of synaptic transmission by shaping the frequency dependence of synaptic responses (Heine et al., 2008). Moreover, the lateral mobility of desensitized GABAA receptors allows a given inhibitory synapse to transfer the ‘‘memory’’ of its latest activation to adjacent inhibitory synapses, acting as a new mechanism of inter-synaptic crosstalk (de Luca et al., 2017).

One of the mechanisms underlying the receptor trapping to the synaptic area is the gephyrin anchoring activity that induces a transient “stop-and-go” behaviour of receptors at the synapse. How protein diffusion influences synaptic plasticity by regulating the availability of synaptic receptors at synapses remains a major challenge in synaptic physiology.

In this work, we address the fine diffusive dynamics of gephyrin in different subcellular zones by means of fluorescence correlation spectroscopy (FCS) and arbitrary region raster image correlation spectroscopy (ARICS). We show here, for the first time, the absolute diffusion coefficients of gephyrin cytoplasmic dynamics in cellular and neuronal environment.

We observe a fast component of “free diffusion gephyrin” in every compartment that probably behaves as a reservoir of diffusing “elementary blocks” for the continuous renewal of gephyrin clusters, in according with the “aggregation-removal model” (Ranft, Almeida, Rodriguez, Triller, & Hakim, 2017). At the same time, we have found that, both in the cytoplasmic space and in

the cluster area, there is a gephyrin population diffusing one thousand times slower than the cytoplasmic fraction, that shows similar diffusion coefficient of GABAA receptor. The slow component in the cytoplasmic space may represent an evidence that the gephyrin-GABAA receptor complex can exist far from the cluster area as reported in 2007 by the Ehrensperger's work (Ehrensperger, Hanus, Vannier, Triller, & Dahan, 2007). Furthermore, we can speculate that the heterogeneous mobility pattern we found in the cluster and in pericluster areas can support the reshaping of inhibitory post-synaptic scaffold cluster in nanodomains of different levels of molecular crowding, resulting in different mobility diffusion range (Pennacchietti et al., 2017).

Experiments performed using the fast-diffusing Gephyrin-delta-2-188 (a mutant form of gephyrin with reduced oligomerization capability, ((Maas et al., 2006) have demonstrated the crucial relationship between the gephyrin diffusion properties and its clusterization state. In fact, both FCS and ARICS measurements have highlighted the increased diffusion coefficient of gephyrin delta in HEK cells, N2a cells and hippocampal neurons. Despite the higher diffusion dynamics, the gephyrin-delta-2-188 displays a significant mobility downturn when expressed in neurons (almost three-fold reduction), respect to the cell lines cellular environment. The same results have been obtained using the monomeric EGFP, highlighting the crucial role of the molecular crowding or shape constraints that modulate the dynamics of synaptic protein.

In another set of experiments, Quantum Dot based SPT has been able to measure the diffusion coefficient of GABAA receptor in extracellular aqueous solution, but when a more viscous solution has been added (extracellular solution + dextran 10% weight/volume) the detected GABAAR diffusion coefficient was significantly lower.

In parallel, FCS approach has been applied also to GABAA receptor to reproduce the results obtained by means of SPT. Nevertheless, the average diffusion measured with FCS has not been affected by the dextran 10% solution, indicating that this approach is suitable to study transmembrane proteins exposed to extracellular conditions that may mimic the viscosity of the extracellular matrix. To check if the detection particles of the QD-SPT may be involved in this

protein downturn, we have performed “hybrid” experiments (FCS+SPT) on GABAA receptor, demonstrating the direct slow down due to the extracellular antibody-QD complex structure that interact with the extracellular environment.

Furthermore, our data demonstrate the significant impact that the “bulky” SPT detection system can exert on receptor lateral mobility (Figure 21), thus raising the point that extracellular domains of transmembrane proteins may hinder the protein diffusion especially in conditions of high extracellular viscosity, that are expected to take place in *ex vivo* brain slices or in *in vivo* environment due to the presence of the extracellular matrix. On the contrary, the FCS confocal nature and its detection system insensitivity to the extracellular viscosity, may provide a technique for further investigation of the protein dynamics in higher complexity *in vivo* environment.

BIBLIOGRAPHY

Barberis, A., Mozrzymas, J. W., Ortinski, P. I., & Vicini, S. (2007). Desensitization and binding properties determine distinct alpha1beta2gamma2 and alpha3beta2gamma2 GABA(A) receptor-channel kinetic behavior. *The European Journal of Neuroscience*, *25*(9), 2726–40. https://doi.org/10.1111/j.1460-9568.2007.05530.x

Barberis, A., Petrini, E. M., & Cherubini, E. (2004). Presynaptic source of quantal size variability at GABAergic synapses in rat hippocampal neurons in culture. *European Journal of Neuroscience*, *20*(7), 1803–1810. https://doi.org/10.1111/j.1460-9568.2004.03624.x

Bartos, M., Vida, I., Frotscher, M., Meyer, A., Monyer, H., Geiger, J. R. P., & Jonas, P. (2002). Fast synaptic inhibition promotes synchronized gamma oscillations in hippocampal interneuron networks. *Proceedings of the National Academy of Sciences*, *99*(20), 13222–13227. https://doi.org/10.1073/pnas.192233099

Bartos, M., Vida, I., & Jonas, P. (2007). Synaptic mechanisms of synchronized gamma oscillations in inhibitory interneuron networks. *Nature Reviews Neuroscience*, *8*(1), 45–56. https://doi.org/10.1038/nrn2044

Belaidi, A. A., & Schwarz, G. (2013). Metal insertion into the molybdenum cofactor : product – substrate channelling demonstrates the functional origin of domain fusion in gephyrin, *157*, 149–157. https://doi.org/10.1042/BJ20121078

Borgdorff, A. J., & Choquet, D. (2002). Regulation of AMPA receptor lateral movements. *Nature*, *417*(6889), 649–53. https://doi.org/10.1038/nature00780

Bormann, J. (2000). The “ABC” of GABA receptors.

Cherubini, E., & Conti, F. (2001). Generating diversity at GABAergic synapses. *Trends in*

Neurosciences, *24*(3), 155–62. Retrieved from http://www.ncbi.nlm.nih.gov/pubmed/11182455

Choii, G., & Ko, J. (2015). Gephyrin: a central GABAergic synapse organizer. *Experimental & Molecular Medicine*, *47*(4), e158. https://doi.org/10.1038/emm.2015.5

Cognet, L., Leduc, C., & Lounis, B. (2014). Advances in live-cell single-particle tracking and dynamic super-resolution imaging. *Current Opinion in Chemical Biology*, *20*(1), 78–85. https://doi.org/10.1016/j.cbpa.2014.04.015

Dawson, G. R., Maubach, K. A., Collinson, N., Cobain, M., Everitt, B. J., MacLeod, A. M., … Atack, J. R. (2006). An inverse agonist selective for alpha5 subunit-containing GABAA receptors enhances cognition. *The Journal of Pharmacology and Experimental Therapeutics*, *316*(3), 1335–45. https://doi.org/10.1124/jpet.105.092320

de Luca, E., Ravasenga, T., Petrini, E. M., Polenghi, A., Nieus, T., Guazzi, S., & Barberis, A. (2017). Inter-Synaptic Lateral Diffusion of GABAA Receptors Shapes Inhibitory Synaptic Currents. *Neuron*, *95*(1), 63–69.e5. https://doi.org/10.1016/j.neuron.2017.06.022

Derkach, V. A., Oh, M. C., Guire, E. S., & Soderling, T. R. (2007). Regulatory mechanisms of AMPA receptors in synaptic plasticity. *Nat.Rev.Neurosci.*, *8*(1471–003X (Print) LA–eng PT–Journal Article PT–Research Support, N.I.H., Extramural PT–Review RN–0 (Receptors, AMPA) SB–IM), 101–113. https://doi.org/10.1038/nrn2055

Di Rienzo, C., Gratton, E., Beltram, F., & Cardarelli, F. (2014). From Fast Fluorescence Imaging to Molecular Diffusion Law on Live Cell Membranes in a Commercial Microscope. *Journal of Visualized Experiments*, (92), 1–12. https://doi.org/10.3791/51994

Ehrensperger, M.-V., Hanus, C., Vannier, C., Triller, A., & Dahan, M. (2007). Multiple Association States between Glycine Receptors and Gephyrin Identified by SPT Analysis. *Biophysical Journal*, *92*(10), 3706–3718. https://doi.org/10.1529/biophysj.106.095596

Fernandes, C. C., Berg, D. K., & Gomez-Varela, D. (2010). Lateral Mobility of Nicotinic Acetylcholine Receptors on Neurons Is Determined by Receptor Composition, Local Domain, and Cell Type. *Journal of Neuroscience*, *30*(26), 8841–8851. https://doi.org/10.1523/JNEUROSCI.6236-09.2010

Flores, C. E., Nikonenko, I., Mendez, P., Fritschy, J.-M., Tyagarajan, S. K., & Muller, D. (2015). Activity-dependent inhibitory synapse remodeling through gephyrin phosphorylation. *Proceedings of the National Academy of Sciences*, *112*(1), E65–E72. https://doi.org/10.1073/pnas.1411170112

Freund, T. F., & Buzsáki, G. (1996). Interneurons of the hippocampus. *Hippocampus*, *6*(4), 347–470. https://doi.org/10.1002/(SICI)1098-1063(1996)6:4<347::AID-HIPO1>3.0.CO;2-I

Gao, B., & Fritschy, J. M. (1994). Selective allocation of GABAA receptors containing the alpha 1 subunit to neurochemically distinct subpopulations of rat hippocampal interneurons. *The European Journal of Neuroscience*, *6*(5), 837–53. Retrieved from http://www.ncbi.nlm.nih.gov/pubmed/8075825

Ghosh, H., Auguadri, L., Battaglia, S., Simone Thirouin, Z., Zemoura, K., Messner, S., … Tyagarajan, S. K. (2016). Several posttranslational modifications act in concert to regulate gephyrin scaffolding and GABAergic transmission. *Nature Communications*, *7*. https://doi.org/10.1038/ncomms13365

Haas, K. F., & Macdonald, R. L. (1999). GABAA receptor subunit gamma2 and delta subtypes confer unique kinetic properties on recombinant GABAA receptor currents in mouse fibroblasts. *The Journal of Physiology*, *514 (Pt 1*, 27–45. Retrieved from http://www.pubmedcentral.nih.gov/articlerender.fcgi?artid=2269054&tool=pmcentrez&rendertype=abstract

Haselwandter, C. A., Calamai, M., Kardar, M., Triller, A., & Azeredo Da Silveira, R. (2011).

Formation and stability of synaptic receptor domains. *Physical Review Letters*, *106*(23). https://doi.org/10.1103/PhysRevLett.106.238104

Heine, M., Groc, L., Frischknecht, R., Béïque, J.-C., Lounis, B., Rumbaugh, G., … Choquet, D. (2008). Surface mobility of postsynaptic AMPARs tunes synaptic transmission. *Science (New York, N.Y.)*, *320*(5873), 201–205. https://doi.org/10.1126/science.1152089

Hendrix, J., Dekens, T., Schrimpf, W., & Lamb, D. C. (2016). Arbitrary-Region Raster Image Correlation Spectroscopy. *Biophysical Journal*, *111*(8), 1785–1796. https://doi.org/10.1016/j.bpj.2016.09.012

Hendrix, J., Schrimpf, W., Höller, M., & Lamb, D. C. (2013). Pulsed interleaved excitation fluctuation imaging. *Biophysical Journal*, *105*(4), 848–861. https://doi.org/10.1016/j.bpj.2013.05.059

Herweg, J., & Schwarz, G. (2012). Splice-specific glycine receptor binding, folding, and phosphorylation of the scaffolding protein gephyrin. *Journal of Biological Chemistry*, *287*(16), 12645–12656. https://doi.org/10.1074/jbc.M112.341826

Hinde, E., Cardarelli, F., Digman, M. a, & Gratton, E. (2010). In vivo pair correlation analysis of EGFP intranuclear diffusion reveals DNA-dependent molecular flow. *Proceedings of the National Academy of Sciences of the United States of America*, *107*, 16560–16565. https://doi.org/10.1073/pnas.1006731107

Jacob, T. C. (2005). Gephyrin Regulates the Cell Surface Dynamics of Synaptic GABAA Receptors. *Journal of Neuroscience*, *25*(45), 10469–10478. https://doi.org/10.1523/JNEUROSCI.2267-05.2005

Kamdar, K. P., Shelton, M. E., & Finnerty, V. (1994). The drosophila molybdenum cofactor gene cinnamon is homologous to three Escherichia coli cofactor proteins and to the rat protein gephyrin. *Genetics*.

Kim, S. A., Sanabria, H., Digman, M. A., Gratton, E., Schwille, P., Zipfel, W. R., & Waxham, M. N. (2010). Quantifying Translational Mobility in Neurons: Comparison between Current Optical Techniques. *Journal of Neuroscience*, *30*(49), 16409–16416. https://doi.org/10.1523/JNEUROSCI.3063-10.2010

Klausberger, T., & Somogyi, P. (2008). Neuronal Diversity and Temporal Dynamics: The Unity of Hippocampal Circuit Operations. *Science*, *321*(5885), 53–57. https://doi.org/10.1126/science.1149381

Kneussel, M., & Betz, H. (2000). Clustering of inhibitory neurotransmitter receptors at developing postsynaptic sites: The membrane activation model. *Trends in Neurosciences*. https://doi.org/10.1016/S0166-2236(00)01627-1

Kowalczyk, S., Winkelmann, A., Smolinsky, B., Förstera, B., Neundorf, I., Schwarz, G., & Meier, J. C. (2013). Direct binding of GABAA receptor β2 and β3 subunits to gephyrin. *European Journal of Neuroscience*, *37*(4), 544–554. https://doi.org/10.1111/ejn.12078

Lanzanò, L., Scipioni, L., Di Bona, M., Bianchini, P., Bizzarri, R., Cardarelli, F., … Vicidomini, G. (2017). Measurement of nanoscale three-dimensional diffusion in the interior of living cells by STED-FCS. *Nature Communications*, *8*(1), 65. https://doi.org/10.1038/s41467-017-00117-2

Lardi-Studler, B., Smolinsky, B., Petitjean, C. M., Koenig, F., Sidler, C., Meier, J. C., … Schwarz, G. (2007). Vertebrate-specific sequences in the gephyrin E-domain regulate cytosolic aggregation and postsynaptic clustering. *Journal of Cell Science*, *120*(8), 1371–1382. https://doi.org/10.1242/jcs.003905

Li, X., Xing, J., Qiu, Z., He, Q., & Lin, J. (2016). Quantification of Membrane Protein Dynamics and Interactions in Plant Cells by Fluorescence Correlation Spectroscopy. *Molecular Plant*. https://doi.org/10.1016/j.molp.2016.06.017

Lisman, J., Yasuda, R., & Raghavachari, S. (2012). Mechanisms of CaMKII action in long-term

potentiation. *Nature Reviews Neuroscience*. https://doi.org/10.1038/nrn3192

Maas, C., Tagnaouti, N., Loebrich, S., Behrend, B., Lappe-Siefke, C., & Kneussel, M. (2006). Neuronal cotransport of glycine receptor and the scaffold protein gephyrin. *Journal of Cell Biology*, *172*(3), 441–451. https://doi.org/10.1083/jcb.200506066

Macdonald, R. L., & Olsen, R. W. (1994). GABAA receptor channels. *Annual Review of Neuroscience*, *17*, 569–602. https://doi.org/10.1146/annurev.ne.17.030194.003033

Magde, D., Elson, E., & Webb, W. W. (1972). Thermodynamic Fluctuations in a Reacting System—Measurement by Fluorescence Correlation Spectroscopy. *Physical Review Letters*, *29*(11), 705–708. https://doi.org/10.1103/PhysRevLett.29.705

Maric, H. M., Kasaragod, V. B., Hausrat, T. J., Kneussel, M., Tretter, V., Strømgaard, K., & Schindelin, H. (2014). Molecular basis of the alternative recruitment of GABAA versus glycine receptors through gephyrin. *Nature Communications*, *5*, 5767. https://doi.org/10.1038/ncomms6767

Mayer, M. L. (2006). Glutamate receptors at atomic resolution. *Nature*, *440*(7083), 456–62. https://doi.org/10.1038/nature04709

McIntire, S. L., Reimer, R. J., Schuske, K., Edwards, R. H., & Jorgensen, E. M. (1997). Identification and characterization of the vesicular GABA transporter. *Nature*, *389*(6653), 870–6. https://doi.org/10.1038/39908

Meier, J., Vannier, C., Sergé, A., Triller, A., & Choquet, D. (2001). Fast and reversible trapping of surface glycine receptors by gephyrin. *Nature Neuroscience*, *4*(3), 253–60. https://doi.org/10.1038/85099

Moerner, W. E. (1999). Illuminating Single Molecules in Condensed Matter. *Science*, *283*(5408), 1670–1676. https://doi.org/10.1126/science.283.5408.1670

Moss, S. J., & Smart, T. G. (2001). Constructing inhibitory synapses. *Nature Reviews. Neuroscience*,

2(4), 240–50. https://doi.org/10.1038/35067500

Mou, L., Dias, B. G., Gosnell, H., & Ressler, K. J. (2013). Gephyrin plays a key role in BDNF-dependent regulation of amygdala surface GABAARs. *Neuroscience*, *255*, 33–44. https://doi.org/10.1016/j.neuroscience.2013.09.051

Mukherjee, J., Kretschmannova, K., Gouzer, G., Maric, H.-M., Ramsden, S., Tretter, V., … Moss, S. J. (2011). The Residence Time of GABAARs at Inhibitory Synapses Is Determined by Direct Binding of the Receptor 1 Subunit to Gephyrin. *Journal of Neuroscience*, *31*(41), 14677–14687. https://doi.org/10.1523/JNEUROSCI.2001-11.2011

Nagy, A., Wu, J., & Berland, K. M. (2005). Observation Volumes and γ-Factors in Two-Photon Fluorescence Fluctuation Spectroscopy. *Biophysical Journal*, *89*(3), 2077–2090. https://doi.org/10.1529/biophysj.104.052779

Nicoll, R. a, Malenka, R. C., & Kauer, J. a. (1990). *Functional comparison of neurotransmitter receptor subtypes in mammalian central nervous system. Physiological reviews* (Vol. 70).

Olsen, R. W., & Sieghart, W. (2009). GABA A receptors: subtypes provide diversity of function and pharmacology. *Neuropharmacology*, *56*(1), 141–8. https://doi.org/10.1016/j.neuropharm.2008.07.045

Owen, D. M., Williamson, D., Rentero, C., & Gaus, K. (2009). Quantitative microscopy: Protein dynamics and membrane organisation. *Traffic*. https://doi.org/10.1111/j.1600-0854.2009.00908.x

Pennacchietti, F., Vascon, S., Nieus, T., Rosillo, C., Das, S., Tyagarajan, S. K., … Cella Zanacchi, F. (2017). Nanoscale Molecular Reorganization of the Inhibitory Postsynaptic Density Is a Determinant of GABAergic Synaptic Potentiation. *The Journal of Neuroscience*, *37*(7), 1747–1756. https://doi.org/10.1523/JNEUROSCI.0514-16.2016

Perrais, D., & Ropert, N. (2000). Altering the concentration of GABA in the synaptic cleft

potentiates miniature IPSCs in rat occipital cortex. *European Journal of Neuroscience*, *12*(1), 400–404. https://doi.org/10.1046/j.1460-9568.2000.00957.x

Petrini, E. M., Lu, J., Cognet, L., Lounis, B., Ehlers, M. D., & Choquet, D. (2009). Endocytic Trafficking and Recycling Maintain a Pool of Mobile Surface AMPA Receptors Required for Synaptic Potentiation. *Neuron*, *63*(1), 92–105. https://doi.org/10.1016/j.neuron.2009.05.025

Petrini, E. M., Ravasenga, T., Hausrat, T. J., Iurilli, G., Olcese, U., Racine, V., … Barberis, A. (2014). Synaptic recruitment of gephyrin regulates surface GABAA receptor dynamics for the expression of inhibitory LTP. *Nature Communications*, *5*, 3921. https://doi.org/10.1038/ncomms4921

Petryayeva, E., Algar, W. R., & Medintz, I. L. (2013). Quantum Dots in Bioanalysis: A Review of Applications across Various Platforms for Fluorescence Spectroscopy and Imaging. *Applied Spectroscopy*, *67*(3), 215–252. https://doi.org/10.1366/12-06948

Qian, H., Sheetz, M. P., & Elson, E. L. (1991). Single particle tracking. Analysis of diffusion and flow in two-dimensional systems. *Biophysical Journal*, *60*(4), 910–21. https://doi.org/10.1016/S0006-3495(91)82125-7

Ranft, J., Almeida, L. G., Rodriguez, P. C., Triller, A., & Hakim, V. (2017). An aggregation-removal model for the formation and size determination of post-synaptic scaffold domains. *PLoS Computational Biology*, *13*(4). https://doi.org/10.1371/journal.pcbi.1005516

Renner, M., Specht, C. G., & Triller, A. (2008). Molecular dynamics of postsynaptic receptors and scaffold proteins. *Current Opinion in Neurobiology*. https://doi.org/10.1016/j.conb.2008.09.009

Schrader, N., Kim, E. Y., Winking, J., Paulukat, J., Schindelin, H., & Schwarz, G. (2004). Biochemical Characterization of the High Affinity Binding between the Glycine Receptor and Gephyrin *, *279*(18), 18733–18741. https://doi.org/10.1074/jbc.M311245200

Sergé, A., Fourgeaud, L., Hémar, A., & Choquet, D. (2002). Receptor activation and homer differentially control the lateral mobility of metabotropic glutamate receptor 5 in the neuronal membrane. *The Journal of Neuroscience : The Official Journal of the Society for Neuroscience*, *22*(10), 3910–20. https://doi.org/20026331

Simson, R., Yang, B., Moore, S. E., Doherty, P., Walsh, F. S., & Jacobson, K. A. (1998). Structural mosaicism on the submicron scale in the plasma membrane. *Biophysical Journal*, *74*(1), 297–308. https://doi.org/10.1016/S0006-3495(98)77787-2

Singer, S. J., & Nicolson, G. L. (1972). The fluid mosaic model of the structure of cell membranes. *Science (New York, N.Y.)*, *175*(4023), 720–31.

Sivilotti, L., & Nistri, A. (1991). GABA receptor mechanisms in the central nervous system. *Progress in Neurobiology*, *36*(1), 35–92. Retrieved from http://www.ncbi.nlm.nih.gov/pubmed/1847747

Sohal, V. S., Zhang, F., Yizhar, O., & Deisseroth, K. (2009). Parvalbumin neurons and gamma rhythms enhance cortical circuit performance. *Nature*, *459*(7247), 698–702. https://doi.org/10.1038/nature07991

Sola, M., Bavro, V. N., Timmins, J., Franz, T., Ricard-Blum, S., Schoehn, G., … Weissenhorn, W. (2004). Structural basis of dynamic glycine receptor clustering by gephyrin. *The EMBO Journal*, *23*(13), 2510–9. https://doi.org/10.1038/sj.emboj.7600256

Sola, M., Kneussel, M., Heck, I. S., Betz, H., & Weissenhorn, W. (2001). X-ray Crystal Structure of the Trimeric N-terminal Domain of Gephyrin. *Journal of Biological Chemistry*, *276*(27), 25294–25301. https://doi.org/10.1074/jbc.M101923200

Somogyi, P., Fritschy, J. M., Benke, D., Roberts, J. D., & Sieghart, W. (1996). The gamma 2 subunit of the GABAA receptor is concentrated in synaptic junctions containing the alpha 1 and beta 2/3 subunits in hippocampus, cerebellum and globus pallidus. *Neuropharmacology*, *35*(9–10),

1425–44. Retrieved from http://www.ncbi.nlm.nih.gov/pubmed/9014159

Spruston, N. (2008)A. Pyramidal neurons: dendritic structure and synaptic integration. *Nature Reviews Neuroscience*, *9*(3), 206–221. https://doi.org/10.1038/nrn2286

Tardin, C., Cognet, L., Bats, C., Lounis, B., & Choquet, D. (2003a)B. Direct imaging of lateral movements of AMPA receptors inside synapses. *EMBO Journal*, *22*(18), 4656–4665. https://doi.org/10.1093/emboj/cdg463

Tardin, C., Cognet, L., Bats, C., Lounis, B., & Choquet, D. (2003b)L. Direct imaging of lateral movements of AMPA receptors inside synapses. *The EMBO Journal*, *22*(18), 4656–65. https://doi.org/10.1093/emboj/cdg463

Thurner, P., Gsandtner, I., Kudlacek, O., Choquet, D., Nanoff, C., Freissmuth, M., & Zezula, J. (2014)A. A two-state model for the diffusion of the a2A adenosine receptor in hippocampal neurons: Agonist-induced switch to slow mobility is modified by synapse-associated protein 102 (SAP102). *Journal of Biological Chemistry*, *289*(13), 9263–9274. https://doi.org/10.1074/jbc.M113.505685

Tovar, K. R., & Westbrook, G. L. (2002)B. Mobile NMDA receptors at hippocampal synapses. *Neuron*, *34*(2), 255–64. Retrieved from http://www.ncbi.nlm.nih.gov/pubmed/11970867

Tretter, V., Jacob, T. C., Mukherjee, J., Fritschy, J., Pangalos, M. N., & Moss, S. J. (2008)I. The Clustering of GABA A Receptor Subtypes at Inhibitory Synapses is Facilitated via the Direct Binding of Receptor ␣ 2 Subunits to Gephyrin, *28*(6), 1356–1365. https://doi.org/10.1523/JNEUROSCI.5050-07.2008

Tyagarajan, S. K., & Fritschy, J.-M. (2014)N. Gephyrin: a master regulator of neuronal function? *Nature Reviews. Neuroscience*, *15*(3), 141–56. https://doi.org/10.1038/nrn3670

Tyagarajan, S. K., Ghosh, H., Yévenes, G. E., Imanishi, S. Y., Zeilhofer, H. U., Gerrits, B., & Fritschy, J. M. (2013)F. Extracellular signal-regulated kinase and glycogen synthase kinase 3β regulate

gephyrin postsynaptic aggregation and GABAergic synaptic function in a calpain-dependent mechanism. *Journal of Biological Chemistry*, *288*(14), 9634–9647. https://doi.org/10.1074/jbc.M112.442616

Tyagarajan, S. K., Ghosh, H., Yevenes, G. E., Nikonenko, I., Ebeling, C., Schwerdel, C., … Fritschy, J.-M. (2011)A. Regulation of GABAergic synapse formation and plasticity by GSK3 -dependent phosphorylation of gephyrin. *Proceedings of the National Academy of Sciences*, *108*(1), 379–384. https://doi.org/10.1073/pnas.1011824108

Vicidomini, G., Coto Hernández, I., D'Amora, M., Cella Zanacchi, F., Bianchini, P., & Diaspro, A. (2014)M. Gated CW-STED microscopy: A versatile tool for biological nanometer scale investigation. *Methods*, *66*(2), 124–130. https://doi.org/10.1016/j.ymeth.2013.06.029

Vicini, S., Ferguson, C., Prybylowski, K., Kralic, J., Morrow, A. L., & Homanics, G. E. (2001)I. GABA(A) receptor alpha1 subunit deletion prevents developmental changes of inhibitory synaptic currents in cerebellar neurons. *The Journal of Neuroscience : The Official Journal of the Society for Neuroscience*, *21*(9), 3009–16. Retrieved from http://www.ncbi.nlm.nih.gov/pubmed/11312285

Thanks to my family.